

Methylome Analysis of Human Bone Marrow MSCs Reveals Extensive Age- and Culture-Induced Changes at Distal Regulatory Elements

Kalyan K. Pasumarthy,^{1,8} Naresh Doni Jayavelu,^{1,2,8} Lotta Kilpinen,³ Colin Andrus,² Stephanie L. Battle,² Matti Korhonen,⁴ Petri Lehenkari,^{5,6} Riikka Lund,^{1,7} Saara Laitinen,³ and R. David Hawkins^{1,2,*}

¹Turku Centre for Biotechnology, University of Turku, Turku 20520, Finland

²Division of Medical Genetics, Department of Medicine, Department of Genome Sciences, Institute for Stem Cell and Regenerative Medicine, University of Washington School of Medicine, Seattle, WA 98195, USA

³Research and Development, Medical Services, Finnish Red Cross Blood Service, Helsinki 00310, Finland

⁴Cell Therapy Services, Medical Services, Finnish Red Cross Blood Service, Helsinki 00310, Finland

⁵Institute of Clinical Medicine, Division of Surgery and Institute of Biomedicine, Department of Anatomy and Cell Biology, University of Oulu, Oulu 90014, Finland

⁶Clinical Research Center, Department of Surgery and Intensive Care, Oulu University Hospital, Oulu 90014, Finland

⁷Åbo Akademi University, Turku 20520, Finland

⁸Co-first author

*Correspondence: rdhawk@uw.edu

<http://dx.doi.org/10.1016/j.stemcr.2017.07.018>

SUMMARY

Human bone marrow stromal cells, or mesenchymal stem cells (BM-MSCs), need expansion prior to use as cell-based therapies in immunological and tissue repair applications. Aging and expansion of BM-MSCs induce epigenetic changes that can impact therapeutic outcomes. By applying sequencing-based methods, we reveal that the breadth of DNA methylation dynamics associated with aging and expansion is greater than previously reported. Methylation changes are enriched at known distal transcription factor binding sites such as enhancer elements, instead of CpG-rich regions, and are associated with changes in gene expression. From this, we constructed hypo- and hypermethylation-specific regulatory networks, including a sub-network of BM-MSC master regulators and their predicted target genes, and identified putatively disrupted signaling pathways. Our genome-wide analyses provide a broader overview of age- and expansion-induced DNA methylation changes and a better understanding of the extent to which these changes alter gene expression and functionality of human BM-MSCs.

INTRODUCTION

Mesenchymal stem cells (MSCs), including bone marrow (BM) stromal cells, are of great therapeutic interest due to their diverse regenerative and immunomodulatory properties (Phinney and Prockop, 2007). Successful MSC therapy requires *in vitro* expansion and the proliferative capacity and lifespan of MSCs vary across donors (Wagner et al., 2010a). The variation in cell divisions before entering the senescent stage (Hayflick limit) may be a result of occasional transient clonal aneuploidies, telomeric shortening, and changes in epigenomic profiles (Bentivegna et al., 2013). Molecular profiling has shed light on the role of epigenetic factors including DNA methylation and microRNAs in cellular senescence of MSCs (Bork et al., 2010; Koch et al., 2012, 2013; Schellenberg et al., 2011). Hypermethylation due to the long-term expansion of cells in culture, at genes related to MSC senescence, DNA replication, cell-cycle and adipogenic differentiation was reported previously (Choi et al., 2012). Senescence-associated DNA methylation changes are enriched in intergenic and non-promoter regions (Koch et al., 2013).

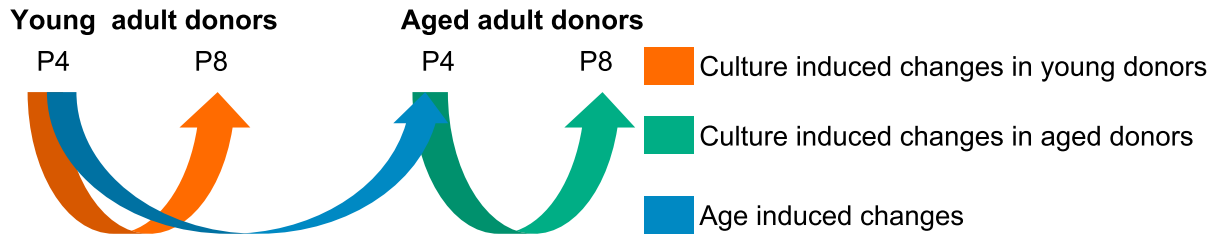
Previous studies in BM-MSCs made significant advancements in determining DNA methylation changes induced by age and expansion of cells in culture using array-based

technologies, but are largely biased toward promoters or CpG-rich regions and with limited CpG representation. Methylation changes at functional elements, such as distal transcription factor binding sites (TFBSs), DNase I hypersensitive sites (DHSs), and enhancer elements, therefore, remain largely unexplored. Moreover, DNA methylation changes specifically at BM-MSC enhancers have not been reported. Studies using high-resolution genome-wide technologies reported that significant methylation changes occur outside of transcription start sites (TSSs) and are predominantly at introns, enhancers, DHSs, and regions with lower CpG densities (Hon et al., 2013; Lister et al., 2009; Staudler et al., 2011). Broadening our view of the DNA methylation landscape in BM-MSCs will reveal additional changes with age and expansion in culture that impact our understanding of cellular aging and ultimately how these cells are maintained and characterized prior to therapeutic use.

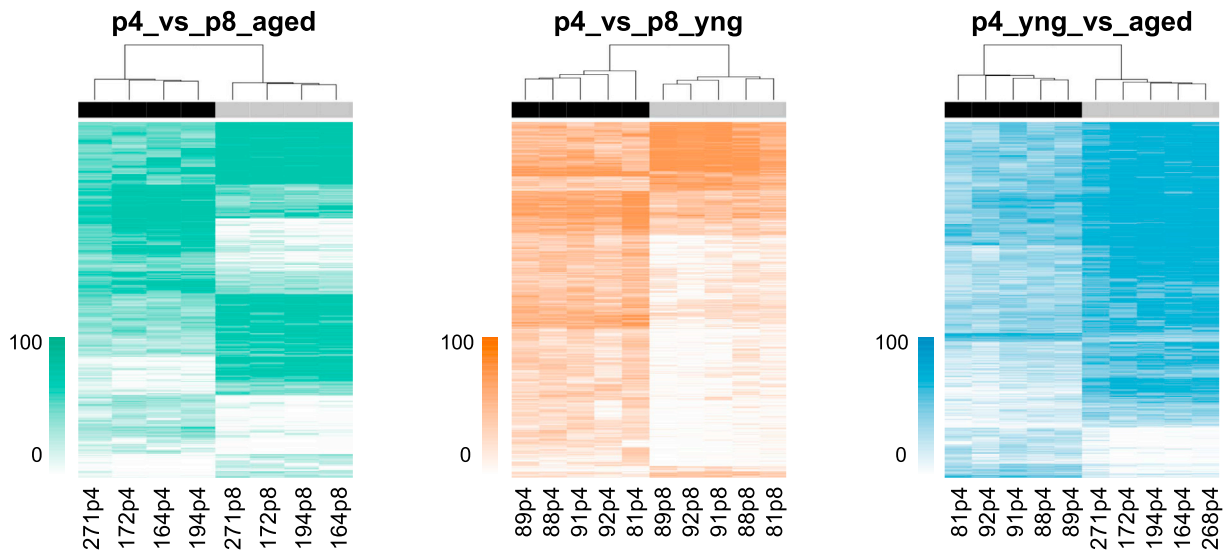
Using enhanced reduced representation bisulfite sequencing (ERRBS), we performed a global DNA methylation profiling across CpG-rich regions along with regions having variable CpG densities and distal regulatory elements from human BM-MSCs from young and aged adults at early and late passages. To further corroborate our findings we performed whole genome bisulfite sequencing (WGBS) on a limited number of BM-MSC donors from young and aged



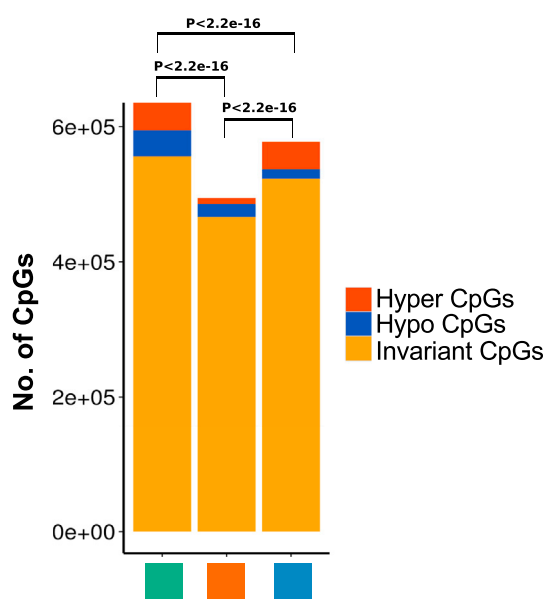
A Schematic Representation of Datasets



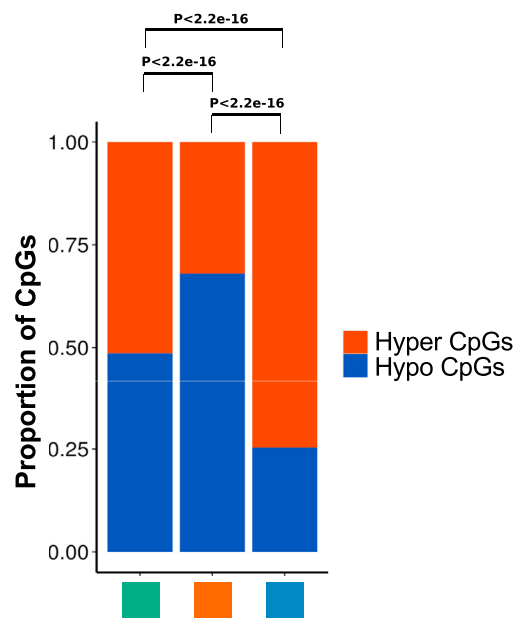
B Heatmaps indicating the methylation status of the CpGs



C Profile of CpGs in each dataset



D Profile of DMCs in each dataset



(legend on next page)



adults at early passage. These high-resolution genome-wide maps in BM-MSCs confirm that distal regulatory elements are highly variable in age-related methylation changes. Through the integration of DNA methylation dynamics with functional elements including enhancers, TFBSs and DHSs we gained a more complete understanding of the influence of DNA methylation on gene expression changes during culture expansion (referred to as “culture-induced”) and biological aging (referred to as “age-induced”).

RESULTS

High-Resolution Global Methylation Analysis of Age- and Culture-Induced Changes

We performed ERRBS to obtain single nucleotide resolution methylation data (Akalin et al., 2012). The methylation status of CpGs from young and aged donors were compared at an early passage (p4) to determine age-associated changes, and culture-induced changes were determined by profiling young and aged donors at passage 4 (p4) and passage 8 (p8) (Figure 1A). Since we have previously generated gene expression data for these samples (Kilpinen et al., 2013), we further focused on the integrative analysis of DNA methylation, gene expression, and additional epigenomic data identifying regulatory elements.

We identified invariant and differentially methylated CpGs (DMCs) between passage- and age-grouped donors (Figures 1B and S1). DMCs were further classified into hyper- and hypomethylated. The majority of CpGs were invariant (Figure 1C). For culture-induced methylation drift, cells from aged donors showed the highest degree of methylation changes (12.6% of CpGs analyzed) with equal proportions of hypo- and hypermethylation (Figures 1C and 1D). Young donors showed minimal changes in methylation (only 5.6% of CpGs analyzed), with the majority of the CpGs exhibiting hypomethylation. In biological aging cells from aged donors gained methylation relative to young donors.

Methylation Changes at Genic Elements

Previous MSC studies reporting methylation changes largely focused on promoter regions. Bork et al. (2010) iden-

tified 84 DMCs in long-term culture and 644 promoter DMCs during aging, assessing 27,000 CpGs. Another study identified 64,142 DMCs during aging, with 70.8% being hypomethylated (Fernández et al., 2014). We overlapped mapped CpGs and DMCs with various genic elements including promoters, first exons, remaining other exons, introns, 5' and 3' UTRs. The gain of methylation in promoters and first exons are usually inversely correlated with gene expression (Brenet et al., 2011). For each comparison, we sampled at least 47% of all promoters and 39% of all first exons (Figure 2A; Table S1). Most CpGs at these elements are not differentially methylated, and, therefore, may not account for the majority of changes in gene expression (Figure 2B; Table S1). The dominant methylation changes are found at introns, other exons, and 3' UTRs when measuring the percentage of DMCs relative to mapped CpGs at these elements (Figure 2B), and this was used to eliminate the bias toward larger representation of genic elements in the genome. Of total DMCs identified in each comparative dataset, 37%–38% are present at intronic elements (Table S1). This may implicate regulatory elements embedded within these elements. A larger number of CpGs were differentially methylated in the aged donors during culture and biological aging, while there were minimal changes in young donors across genic elements (Figure 2B; Table S1). This trend continues when assessing other elements (see below), and suggests that the methylomes of young donors are more refractory to culture-induced changes.

Methylation Changes Are Inversely Proportional to CpG Density

CpG density is highest at CpG islands (CGIs) and decreases moving outward from CGIs to shores, shelves, and then open seas (intergenic regions). As expected, we have more mapped CpGs at CGI covering 68.5%–71.9% of total CGIs, followed by 34%–41% of total shores and 11%–18% of total shelves in each comparison (Figure 2C). Although differential methylation was observable at all CGI-related elements, the percentage of DMCs to CpGs mapped was highest in shelves (11.73%–18.12%) followed by shores (6%–14.16%) and least in CGIs (1.71%–6.69%). Similar observations were reported previously in other cell types

Figure 1. Schematic Representation of Datasets and Methylation Status in MSCs

(A) BM-MSCs from multiple donors were grouped into three subsets to evaluate culture-induced changes and biological aging: p4_vs_p8_aged indicates the comparison of early and late passage groups of MSCs from aged donors (green). p4_vs_p8_yng indicates the comparison of early and late passage group of MSCs from young donors (orange). p4_yng_vs_aged indicates the comparison of differences between young and aged adult donors at early passages (blue). These colors are used throughout.

(B) Heatmaps of top 20% most differentially methylated CpGs in each dataset showing each donor and passage.

(C) Number of CpGs captured in each dataset as: invariant (yellow), hyper- (red), and hypomethylated (blue). The proportion of invariant CpGs and variant CpGs (DMCs) are different across the three comparisons and statistically significant.

(D) The proportions of hyper- and hypomethylated CpGs of each datasets. The proportion of hyper and hypo DMCs significantly vary across the three comparisons. The p values are computed using Fisher's exact test. See also Figure S1.

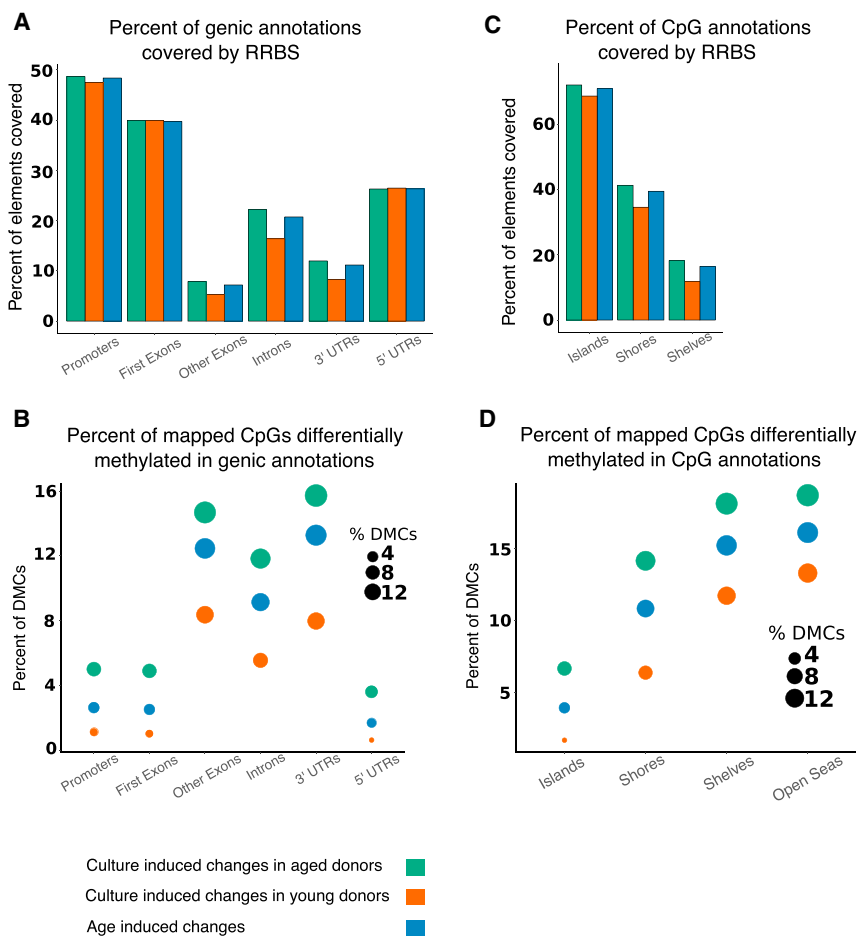


Figure 2. Distribution of Differential Methylation across Genic and CpG Annotation Elements

Bar plot indicates the percent of (A) genic elements or (C) CpG annotation elements mapped to total elements present in the genome in the three datasets. Bubble plot indicates the differential methylation enrichment as percent of DMCs to mapped CpGs overlapping genic elements (B) or CpG annotation elements (D). See also Figure S2, and Tables S1, S2, and S3.

(Irizarry et al., 2009; Sandoval et al., 2011). The differential methylation at open seas was at least twice that of CGIs (Figure 2D). We observed that CpGs proximal to TSSs, such as at promoters, first exons and 5' UTRs are relatively invariant across comparisons, as opposed to CpGs at introns, 3' UTRs and especially open seas (Figures 2B, 2D, and S2). While CGIs are highly represented relative to distal regions in ERRBS, the shelves and open seas contain a higher proportion of DMCs. This suggests that distal regulatory elements may be more susceptible to culture- and age-associated methylation changes. The enrichment of DMCs at various annotations (Figure 2) are statistically significant as opposed to expected by chance ($p < 0.001$; see Table S3 for individual p values). Differential methylation across CGIs, shores, and shelves once again indicated that a larger number of CpGs were altered in aged donors during culture or biological aging compared with young donors (Figures 2B and 2D; Table S2).

DNA Methylation Dynamics at Known TFBSs

DNA methylation at TFBSs can determine the binding of TFs at their sequence motifs, i.e., DNA methylation is either

occlusive or facilitative for the binding of TFs (Blattler and Farnham, 2013), which in turn might affect gene expression. To investigate the overlap with TFBSs, we collected TFBS data from ENCODE only for TFs that are expressed in human BM-MSCs (ENCODE Project Consortium et al., 2012). Because these TFBSs are derived from different cell types, each site may not be bound in BM-MSCs due to differences in chromatin structure; however, this analysis aids in distinguishing DMCs with a potential to affect gene expression. TFBSs were conspicuous at regions harboring differential methylation. Among the culture-induced comparisons, 41% of hypermethylated DMCs from aged donors and 47% from young donors overlapped TFBSs. Age-induced hyper- and hypomethylation changes overlap TFBSs in equal proportions (Figure 3A). Among DMCs overlapping TFBSs, ~34%–35% are within enhancers.

Lastly, we asked which TFs are enriched at DMCs to gain insight on the potential disruption of regulatory networks. The overlap between DMCs and TFBSs was utilized to calculate statistical significance in the overlap with differential methylation (Figures 3B and 3C). We identified a



list of 15,500–77,490 TFBSs that overlap DMCs for culture- and age-induced methylation changes (Figures 3B and 3C; Table S4). These included TFBSs for SIRT6, SMC3, SMARCB1, CHD1, FOSL1, SMARCC2, E2F6, and others that were exclusively hypermethylated in aged donors during culturing (p4_vs_p8_aged); TFBSs for SMARCC1, STAT5, ZNF274, NFE2, JUNB, and others were hypermethylated uniquely during biological aging (p4_young_vs_aged); TFBSs for ZNF143, HSF1, MEF2C, and others were hypermethylated during biological aging and reinforced in aged samples during culture (Figure 3B; Table S4). Among the hypomethylated sites, TFBSs for NR3C1, RCOR1, SP1, ARID3A, and others were hypomethylated in aged donors during culture, and sites belonging to REST and ZBTB33 were hypomethylated during biological aging (Figure 3C; Table S4). Even though we were not able to identify hypermethylated TFBSs specific to young donors, TFBSs for STAT3 and MAFF were hypomethylated specifically during cell culture.

Many of the TFBSs differentially methylated in various comparisons play a role in chromatin structure: SMARCs, SIN3A, EP300, SIRT6, ZBTB33, REST, and SUZ12; or 3D genome architecture: CTCF, RAD21, and SMC3, members of the cohesin complex. These factors suggest that additional means of epigenetic misregulation are at play in the impairment of BM-MSC function during culture and biological aging. Other TFs control key capabilities of MSCs that make them of therapeutic interest. STAT2, which is hypermethylated during biological aging, and also during cell culture in aged donors, is required for the suppression of T cells (Yi et al., 2012). The putatively disrupted binding of STAT2 is likely illustrative of how DNA methylation contributes to the diminishing functionality of BM-MSCs. Hypomethylation at REST and ZBTB33 sites during culturing of aged donor cells may eventually result in aberrant expression of epigenetically repressed genes. ZBTB33 is known to be a DNA methylation-dependent transcriptional repressor that recruits the CoREST chromatin repressive complex (Prokhortchouk et al., 2001). Overall, the enrichment of DMCs at distal TFBSs relative to promoter binding sites (Figure 3D) indicates that previous studies that were focused on promoter or CGI methylation analysis largely underestimated the contribution of distal regulatory elements, and that a whole-genome analysis is needed for a complete understanding of age-associated DNA methylation changes and its impact on gene expression.

Culture-Induced Changes Irrespective of Age

To determine the influence of culture on BM-MSCs, we grouped samples from young and aged donors into early and late passages. We observed that culture-induced methylation changes, irrespective of age, are relatively

minimal across any genomic location; however, 14,482 culture-induced DMCs are shared across age groups accounting for half of the 28,013 culture-induced changes among young donors, and one-fifth of the 79,796 DMCs observed in aged donors (Table S5). This indicates that a majority of methylation changes are specific to either young donors or aged donors, with a subset specific to long-term culture irrespective of adult donor age. Collectively, these results provide the most comprehensive assessment of culture-induced DNA methylation changes. These additional sites may serve as biomarkers of epigenetic drift in both a universal and age-specific manner.

WGBSs in Young and Aged Donors

We employed WGBSs in four donors to facilitate the discovery of methylation changes at all potential regulatory elements. A genome-wide overview indicated that there are substantial differences between aged and young donor samples (Figure 4A). We identified 983,831 hypermethylated CpGs and 976,633 hypomethylated CpGs with age across the genome (Figure 4B). The distribution of hyper- and hypomethylated DMCs was similar across various genomic annotations (Figure 4C). We determined if DMCs directly overlapped regulatory elements by assessing ENCODE TFBSs for factors expressed in BM-MSCs. We found that 226,974 DMCs directly overlap TFBSs ($p < 0.001$). Given that this is a limited set of binding sites, we also included 1,968,675 ENCODE DHSs from human cell types as putative binding sites in BM-MSCs. We reasoned that (1) although these DHSs were not mapped in BM-MSCs, previous studies showed substantial overlap across cell types (Thurman et al., 2012); and (2) the loss of methylation at a known DHSs might create a binding opportunity that could alter gene expression. We found that 401,646 DMCs directly overlap DHSs ($p < 0.001$). To ensure that some TFBSs and DHSs from ENCODE data are likely active binding sites in BM-MSCs, we also overlapped these sites with BM-MSC H3K4me1 enhancer peaks. A recent study using 450,000 methylation arrays found that age-associated hypomethylation often occurred at H3K4me1-marked enhancers from 10 non-MSC cell types (Fernández et al., 2014). We utilized enhancer data generated previously from human BM-MSCs (Roadmap Epigenomics Consortium et al., 2015), representing the first assessment of DNA methylation dynamics at BM-MSC enhancers. WGBS data revealed that H3K4me1-marked BM-MSC enhancers harbor 230,619 DMCs. Of these, 67,779 were directly overlapping known binding sites (TFBSs from chromatin immunoprecipitation sequencing or DHSs). Figure 4D illustrates that DMCs at either TFBSs or DHSs are more enriched at enhancers than other regulatory elements ($p < 0.001$), further illustrating the point that distal regulatory elements are a critical aspect of age-associated

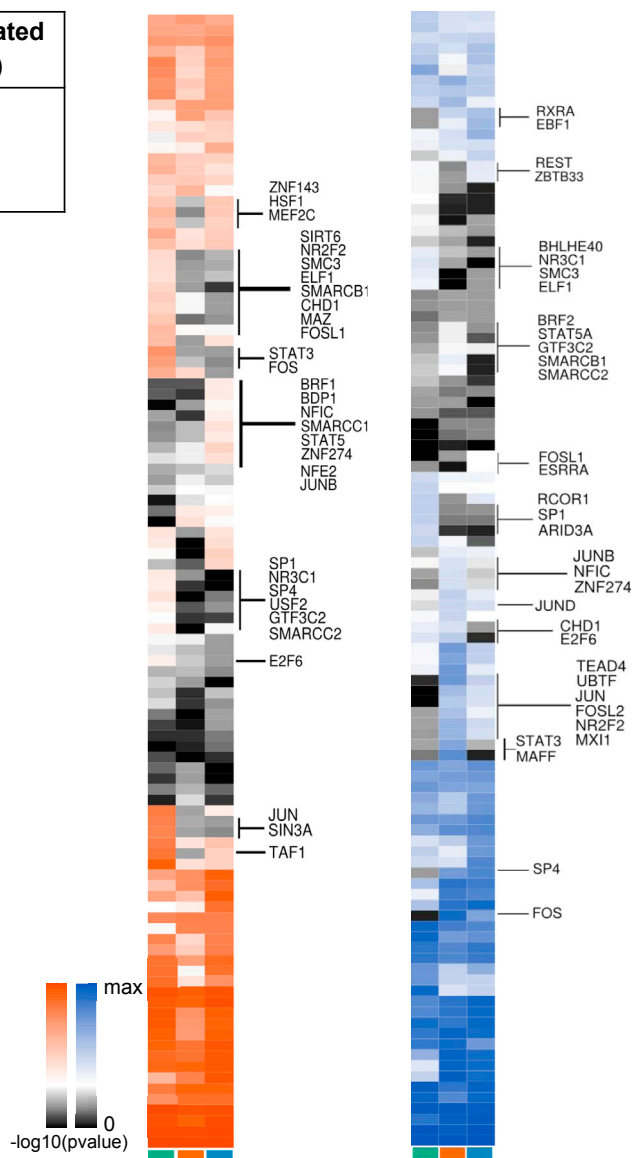


A DMCs Overlapping TFBS

	Hypermethylated CpGs (%)	Hypomethylated CpGs (%)
p4_vs_p8_aged	41.02	35.10
p4_vs_p8_yng	47.73	23.53
p4_yng_vs_aged	36.53	35.03

B Hyper CpGs

C Hypo CpGs



D Distribution of DMCs overlapping at TFBS across genomic annotations of interest

	Hypermethylated CpGs (%) overlapping TFBS at			Hypomethylated CpGs (%) overlapping TFBS at		
	promoters	introns	intergenic regions	promoters	introns	intergenic regions
p4_vs_p8_aged	14.29	0.94	31.24	13.54	1.09	31.66
p4_vs_p8_yng	11.60	1.08	30.84	7.07	1.18	40.50
p4_yng_vs_aged	11.20	1.05	33.03	7.70	0.97	36.89

(legend on next page)



changes in gene expression, and far more extensive than previously reported.

Identification of Age-Associated Differentially Methylated Regions

We identified clusters of DMCs called differentially methylated regions (DMRs). DMRs provide evidence of more sweeping changes within a region. In total, we identified 7,378 DMRs of which 3,809 DMRs are hypermethylated and 3,569 DMRs are hypomethylated (Figure 5A). CpG density at DMRs range from 3 to 132 and their widths span from 5 to 2,894 bp (Figure 5B). The majority of DMRs overlap introns and intergenic regions (Figure 5C). We observed that DMRs overlapping promoters, first exons, other exons, CGIs, DHSs, enhancers, and TFBSs are more likely to be hypermethylated except for CpG shelves, which are largely hypomethylated (Figure 5D). We found 78% and 57% of DMRs are significantly enriched ($p < 0.0001$) with DHSs and enhancers, respectively. Of all DMRs overlapping enhancers, 66% are hyper DMRs. The gain of methylation at these elements is likely to decrease expression of the target genes. While active enhancers generally exhibit hypomethylation, the further loss of DNA methylation with age may result in additional TF binding and increased expression of target genes. Finding fewer DMRs at enhancers compared with DMCs is likely due to enhancers containing very few CpGs (Hon et al., 2013). DMRs occurring outside of regulatory elements may be occurring due to the lack of any regulatory constraint that would otherwise prevent the spreading of the methylation pattern over time.

DMRs occurring at enhancers are often near genes that exhibit an expected corresponding change in gene expression. We have included putative enhancer DMR-gene interactions to further guide which DMR is directly regulating gene expression. These interaction data were obtained from Sheffield et al. (2013), which are based on the correlation of DHS signal intensity with gene expression across numerous cell types. For example, we found the *HOXA* and *HOXB* gene clusters to contain several hyper DMRs overlapping enhancers (Figures 5E and S3; Table S6). Our gene expression data revealed the altered expression of *HOX* genes correlating with observed methylation changes. We found lower expression of *HOXA3*, *HOXA5*, *HOXA6*, *HOXB2-B5*, *HOXB7*, and *HOXC4* in aged donors compared with young donors (Figure 5F). *HOX* gene expression and its adaptation in cell and tissue transplantation may play a role concerning regenerative potential

(Leucht et al., 2008). In addition, we showed previously that the fatty acid desaturases *FADS1* and *FADS2* were downregulated in aged donors, and are important contributors to BM-MSC lipidomic regulation (Kilpinen et al., 2013). This gene cluster also contains DMRs overlapping regional enhancers (Figure S3), indicative of how these genes are likely downregulated via epigenetic repression with age and results in an age-related decline in membrane integrity.

Association of Differential Methylation and Differential Gene Expression

We asked if hyper- or hypomethylation can be associated with differential gene expression previously reported in these samples (Kilpinen et al., 2013). Using the WGBS data for biological aging and ERRBS data for culture-induced comparisons, we identified corresponding changes in gene expression. Among the three comparisons, cells from aged donors (in both culture-induced changes and biological aging) demonstrated a higher number of genes with decreased gene expression levels, whereas cells from younger donors have more genes with increased expression levels. We noticed only a minimal number of differentially methylated promoters showed an inverse relationship with differentially expressed genes (DEGs), 9.41% and 2.87% in culture-induced changes from aged and young donors, respectively, and 5.41% with DMRs and 23.08% with DMCs in biological aging based on WGBS data. A similar trend was observed for an inverse relationship for first exons, 6.79% and 1.72% for culture-induced changes, and 3.4% and 6.9%, respectively, for ERRBS and WGBS age-associated changes. These associations are in line with previous observations where all gene expression was not always inversely correlated with differential methylation (Wagner et al., 2014). Altogether, differential methylation at promoters and first exons explains only a small fraction of culture- or age-induced gene expression changes (Figures 6A–6C). Most of these DEGs are BM-MSCs specific and unique to culture expansion and biological aging (Figure S4). We confirmed this with previously published gene expression data from BM-MSCs (Roson-Burgo et al., 2014) and a well-known stem cell gene list (Müller et al., 2008). Next, we determined if changes in methylation around CpG annotation elements are related to the changes in the nearest neighboring gene (NNG) expression. When increased methylation occurred at CGIs, shores, and shelves, genes associated with them have decreased expression. Overall, the association of

Figure 3. Identifying Differentially Methylated TFBSs

(A) Percentage of DMCs overlapping TFBSs.

(B and C) Heatmaps of $-\log_{10}$ of Fisher's exact p values for TFs with significant hypermethylation (B) or hypomethylation (C).

(D) Distribution of DMCs that overlap TFBSs at promoters, introns, and intergenic regions. See also Table S4.

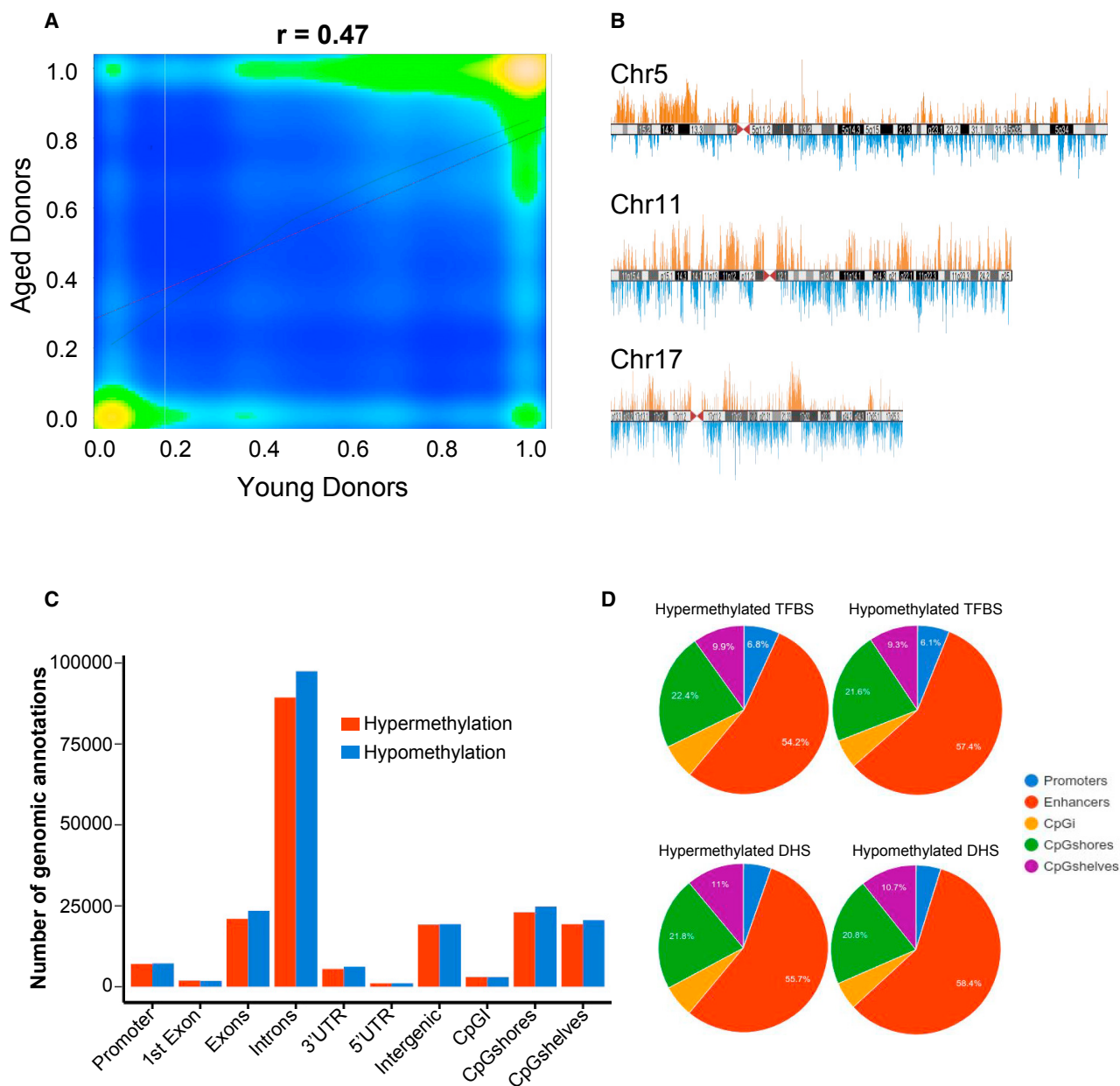


Figure 4. Whole-Genome Methylation Profiles for Biological Aging

(A) Correlation plot showing the methylation differences among the aged and young donors. Correlation was assessed after merging data from two donors per group.

(B) Representative chromosomal ideograms of hyper- (red) and hypomethylation (blue) DMCs on chromosomes 5, 11, and 17.

(C) Distribution of differential methylation at various genomic annotations.

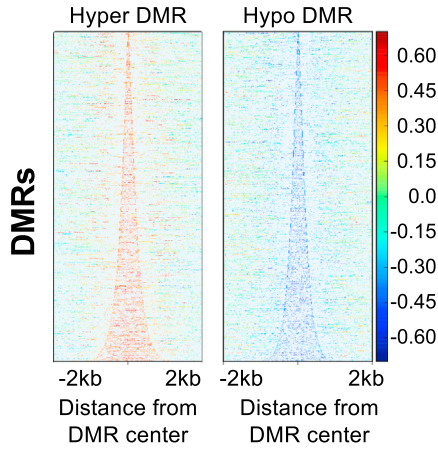
(D) Differential methylation was assessed at binding sites for TFs expressed in MSCs and at DHSs. Pie charts display the distribution of differential methylation at genomic elements that also overlap TFBSs and DHSs.

methylation changes with gene expression was higher with CGI-related elements of the genome (4.6%–16.7% for CpG islands, 6.9%–10.6% for CpG shores, and 1.15%–4.7% for CpG shelves) than with promoters and first exons (Figures 6A–6C).

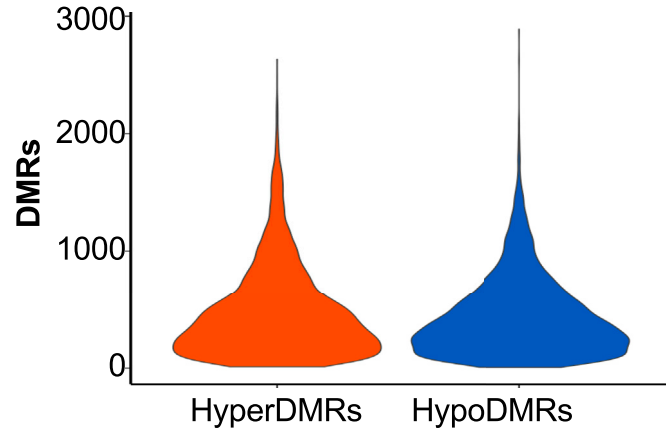
Lastly, we determined if DMCs at TFBSs modulate gene expression for each comparison. DMCs at TFBSs exhibit high variability in terms of methylation changes relative to discrete genomic elements. For example, there is only ~1% of hypermethylated CpGs at intronic TFBSs and



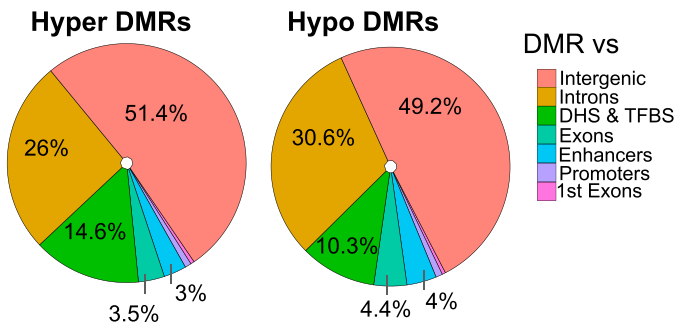
A DMRs across the genome



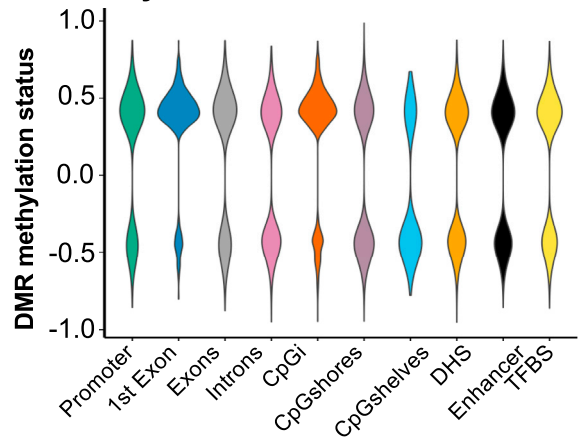
B Width of DMRs across the genome



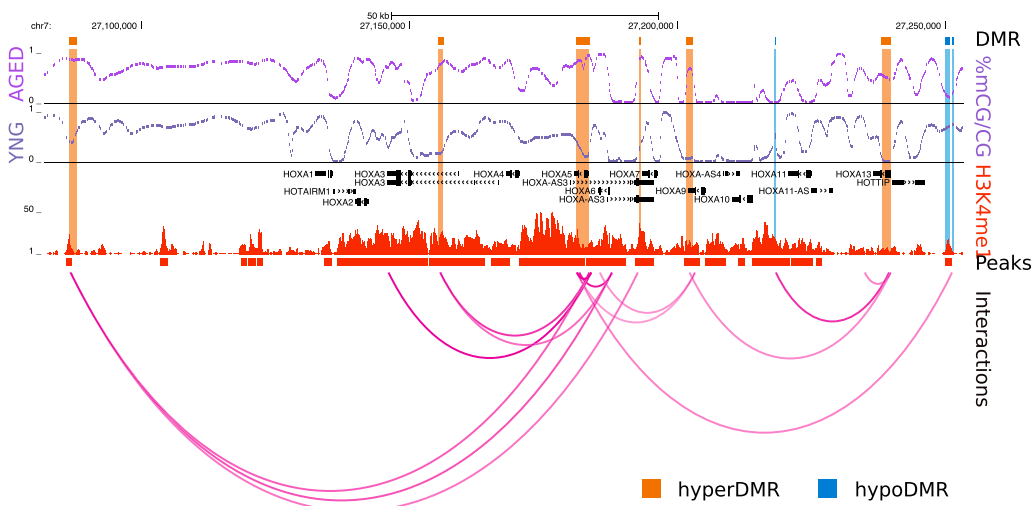
C Distribution of DMRs



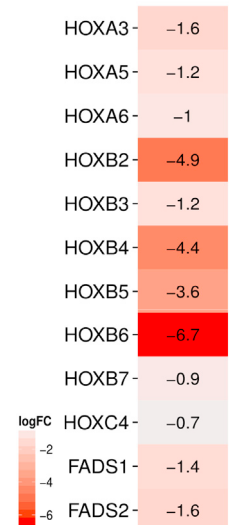
D Methylation status of DMRs



E DMRs at enhancer elements within gene clusters



F Heatmap



(legend on next page)



more than 31% of hypermethylated CpGs at intergenic TFBSs (Figure 3D). We observed similar overlapping patterns with hypomethylated CpGs at introns and intergenic regions (Figure 3D). Previous studies showed that TFBSs (DHSs and chromatin-marked enhancers) within introns of transcribed genes are largely unmethylated, suggesting an inverse correlation with expression (Blattler et al., 2014; Stergachis et al., 2013). We determined if an inverse correlation existed with differentially methylated TFBSs and NNGs. Among DEGs, 8.69% are associated in an inverse manner with DMRs and 53.7% with DMCs identified from WGBS for biological aging. For culture-induced changes, 12.64%–28.04% of genes could be associated with methylation dynamics at neighboring TFBSs (Figure 6).

Transcriptional Regulatory Networks in MSCs

Similar to the ERRBS analysis, we identified TFBSs significantly overlapping with either hyper- or hypomethylated CpGs from WGBS data. Although the majority of TFBSs exhibit both hypo- and hypermethylated CpGs, a few TFs are uniquely enriched for either of them (Figure 7A; Table S7). For instance, CTCF, SUZ12, EP300, MYC, MAX, SRF, and others are enriched for both conditions, while SP1, FOS, FOSL1, and RXRA are uniquely hypermethylated, and PBX3, MAFK, RUNX3, and YY1 are uniquely hypomethylated. These results provide insight on regulatory networks that are disrupted due to age-associated methylation changes.

To better understand the gene-regulatory effect of TFBSs significantly enriched for DMCs, we constructed *in silico* transcriptional networks of TFs and their putative interactions with DEGs. We identified DEGs with promoters overlapping hyper- and hypomethylated TFBSs, and we termed these DEGs as direct targets of TFs. Next, we found the NNG for all distal TFBSs and termed these DEGs as indirect targets. We included only down- and upregulated DEGs for hyper- and hypomethylated TFBSs as targets, respectively. In this manner, we constructed two networks: (1) TFs with hypermethylated CpGs and downregulated DEGs (hyper network); and (2) TFs with hypomethylated CpGs and upregulated DEGs (hypo network) (Figures 7B and S5).

The hyper network includes 287 nodes (89 TFs and 198 DEGs) and 1,307 interactions (262 direct and 1,045

indirect connections), while the hypo network includes 223 nodes (82 TFs and 141 DEGs) and 926 interactions (250 direct and 676 indirect connections). Both networks followed a power law degree distribution, a typical property of regulatory networks. We found that 80% (1,045/1,307 hyper network) and 73% (676/926 hypo network) of interactions were indirect regulation of methylated TFBSs. To further strengthen this observation, we computed these indirect (or distal) interactions for the top 100 DEGs (based on fold change) and found 68.4% (182/266) and 53.3% (104/195) were distal regulatory connections in the hyper and hypo networks, respectively. Thus, the DNA methylation changes observed at distal TFBSs are likely key contributors to altered gene expression.

A recent assessment of gene expression and network analysis of human BM-MSCs and placental MSCs identified a set of MSC master TFs (Roson-Burgo et al., 2014). We extracted a sub-network with these master TFs from the hyper network to find age-associated MSC regulators. This sub-network comprised MYC, MAX, SP1, EGR1, NFYA, and NFYB (Figure 7C), and exhibited 24,878 TFBSs putatively disrupted due to gain of DNA methylation, and 25,584 binding sites potentially gained through hypomethylation.

These master TFs play key roles in the regulation of many critical features of MSCs as cellular therapeutics. MYC is associated with cell proliferation, differentiation, and cell-cycle processes in MSCs (Bhandari et al., 2011). SP1 is known to modulate adipose lineage differentiation in human MSCs (Ruiz de Eguino et al., 2012). NFYA regulates the transcription of the *HOX4* genes by activating numerous pathways related to maintenance and proliferation (Zhu et al., 2005). Gene ontology analysis on the MSC master regulators sub-network identified biological terms related to lipid and fatty acid metabolism (Figure 7D). Previously, we showed that phospholipid and fatty acid profiles change with age and culturing, and were key to the associated decline of human BM-MSC cell membrane and immunomodulatory function (Kilpinen et al., 2013). Age-associated DNA methylation changes at TFBSs for these factors provide new regulatory insights on the declining function of BM-MSCs with age.

Figure 5. DMR Analysis

- (A) Heatmaps showing the difference in CpG methylation values at hyper and hypo DMRs in aged relative to young donors.
- (B) Violin plots representing the width of DMRs.
- (C) Distribution of hyper and hypo DMRs across genomic annotations.
- (D) Violin plot showing the distribution of methylation status of DMRs across the genomic annotations.
- (E) Browser shot of *HOXA* gene cluster illustrating percent methylation levels, H3K4me1-marked enhancers and peaks, DMRs at enhancer elements within gene clusters, and their putative interactions with target genes.
- (F) Heatmap showing the differential gene expression values for *HOXA*, *HOXB*, *HOXC*, and *FADS* genes downregulated with age. See also Figure S3 and Table S6.

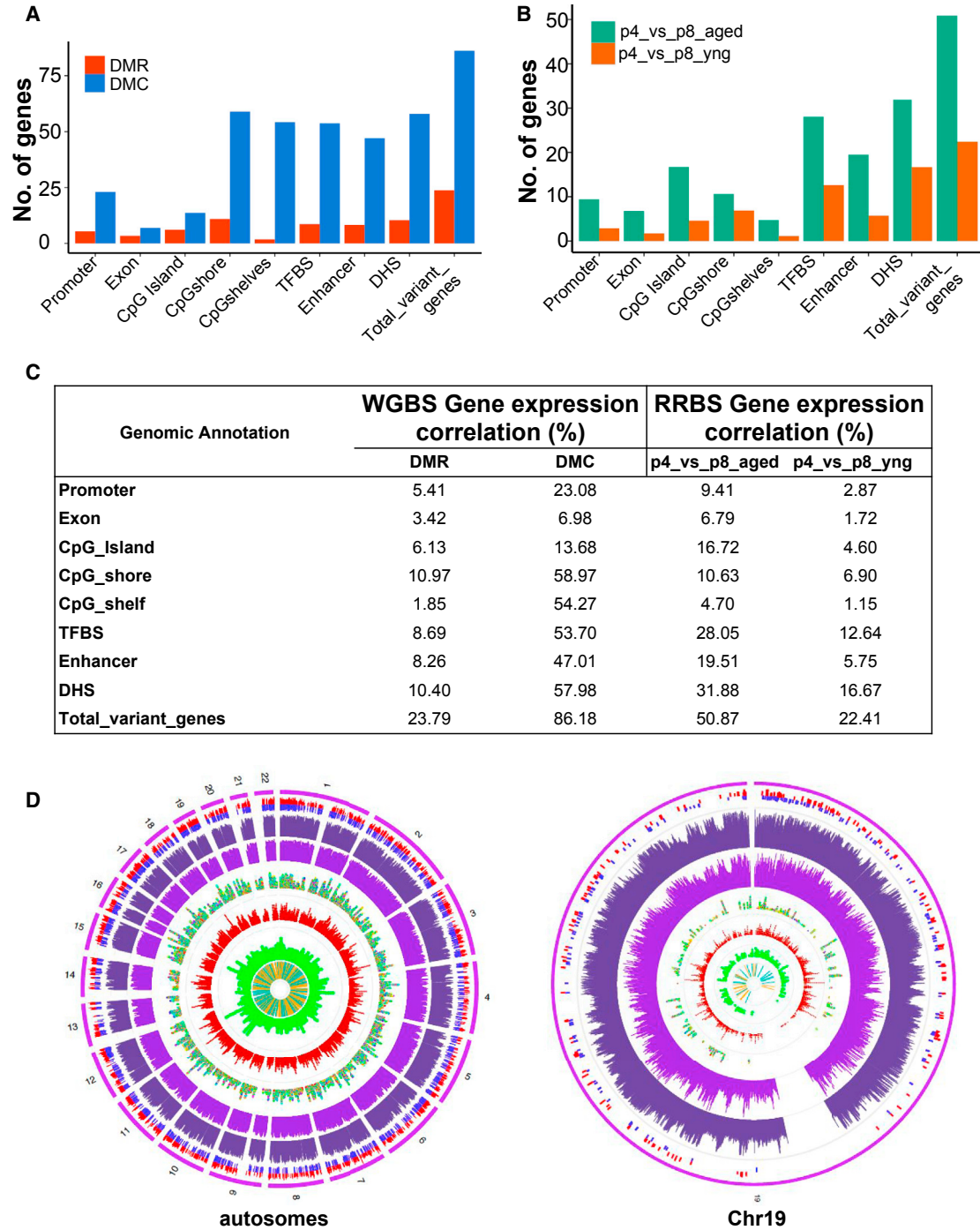


Figure 6. Gene Expression Inverse Correlation with Methylation Data

(A) Number of differentially expressed genes with an inverse corresponding age-associated DNA methylation change at nearest neighboring elements. DMCs and DMRs from WGBS (p4_yng_vs_aged) are shown. Exons are only first exons.

(B) Number of differentially expressed genes with an inverse corresponding DNA methylation changes at nearest neighboring elements from ERRBS data for culture-induced DMCs. Exons are only first exons.

(C) Percentage of gene expression anti-correlated with the differentially methylated genomic elements.

(D) Circos plots providing a genome-wide (left) and chr19 (right) view of expression and epigenomic modifications. From inside to out: (1) orange and blue bars for up- and downregulated genes with age; (2) green stacked dots for DHSs (higher stack = more dense); (3) red

(legend continued on next page)



Identification of Enriched Pathways

Several enriched pathways were identified in both hyper and hypo networks, including osteoclast differentiation, cell-cycle, tumor necrosis factor (TNF), and MAPK signaling pathways (Figure 7E). WNT and ErbB signaling pathways were specific to the hyper network, while JAK-STAT signaling pathway was specific to the hypo network (Figures 7E and 7F). We also identified affected pathways for culture-induced methylation changes from ERRBS data (Figure S6). Transcriptional misregulation in osteoclast differentiation and TNF signaling were enriched in young and aged donors. WNT, MAPK, transforming growth factor β and adipocytokine signaling pathways, and cell-cycle signaling were unique to culture-induced changes in aged donors. There is no single pathway explicitly enriched in culture-induced changes of young donors, which may be reflective of fewer systematic culture-induced changes in young donors.

The enriched pathways are involved in aging of various stem cells, which may extend to MSCs. The decline of WNT signaling due to aging is associated with decreased neural progenitor cell function (L'Episcopo et al., 2014), and with decline in intestinal stem cell regenerative capacity (Nalapareddy et al., 2017). The JAK-STAT signaling has a known role in aging of other tissues, such as a crucial role in impairment of muscle regeneration in satellite cells during aging (Price et al., 2014; Tierney et al., 2014). Collectively, the misregulation of these pathways and others shown in Figure 7E can be explained, in part, through DNA methylation dynamics, and by in large, through changes that occur at distal regulatory elements.

DISCUSSION

Prior to clinical studies MSCs undergo *in vitro* expansion. During expansion, MSCs gradually lose proliferative capacity and secretive properties (Kilpinen et al., 2013; Wagner et al., 2010b), resulting in limited clinical successes (Kim and Cho, 2015). We attempted to narrow the gaps in our understanding of the epigenetic regulation of induced changes due to age and expansion in culture by broadening our view of the extent to which DNA methylation is involved. Global DNA methylation profiles in BM-MSCs from young and aged adult donors identified age-specific differences following cell expansion. Young donors followed a general trend of hypomethylation and overall demonstrated less variation. Pathway analysis revealed that aged donor cells in culture are specifically enriched

for “hyper pathways,” based on hypermethylated TFBSs and associated downregulated genes that include mismatch repair and cell-cycle pathways. These pathways were not enriched in the young donors. Young donors lacked any age-specific pathway enrichment following expansion, meaning any enriched pathways were not unique to young donors. This may explain the refractory nature of younger donor BM-MSCs to replicative senescence in culture. Shifts in age-related and culture-induced methylation changes have important implications on the extent to which donor BM-MSCs should be expanded.

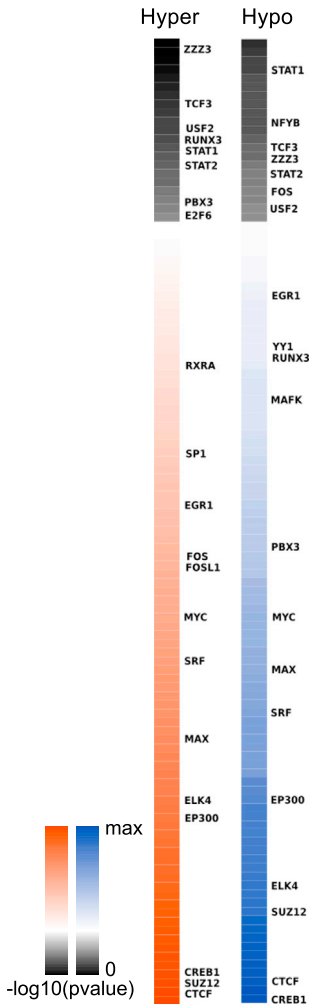
Our genome-wide assessment of methylation changes (WGBS) revealed that age-associated changes are 30 times more extensive than recent array-based studies in BM-MSCs, which identified just over 64,000 DMCs (Fernández et al., 2014). Although WGBS data were generated on limited donors, they provide a first glimpse of DNA methylation changes associated with age on a genome-wide scale. Such epigenomic alterations often influence gene expression and ultimately cellular properties. We found that DNA methylation was more dynamic at distal regulatory elements and accounted for a large increase in the inverse correlation for corresponding changes in gene expression. This included TFBSs for known MSC master regulators (Rosson-Burgo et al., 2014). DNA methylation changes occurring at known TFBSs were most abundant at BM-MSC H3K4me1-marked enhancers, which has not been examined previously. Differential methylation was also frequent at TFBSs for factors involved in the regulation of chromatin structure and 3D genome architecture. One key chromatin modifier was SIRT6, a histone deacetylase with a known role in aging and lifespan (Kanfi et al., 2012). Differential methylation at TFBSs are likely to result in relocalization of these transcription factors and chromatin remodelers in either an occlusive or facilitative manner, and have an impact on chromatin and 3D structures, which are known to be involved in replicative senescence (Hänzelmann et al., 2015).

Induced DNA methylation drift from expansion in culture and aging is bimodal as it involves hyper- and hypomethylation events. Recent studies of DNA methylation changes with age found that DNA methylation profiles become more divergent with age (Boks et al., 2009; Heyn et al., 2012; McClay et al., 2014). BM-MSC differential methylation was three times more prevalent between aged donors than between young donors in our ERRBS data; however, age- and culture-induced changes are not entirely stochastic as demonstrated by the concordance between donors and identification of significantly different

stacked dots for H3K4me1 peaks; (4) stacked dots for TFBSs with each color being a different TF; (5) lighter purple bars with height as average CpG methylation percentage over 500 kb, and 10 kb windows for whole genome and chromosome 19, respectively, for aged donors; (6) darker purple bars showing same type of data as previous track for young donors; (7) DMRs (hyper in red; hypo in blue); (8) chromosome(s). See also Figure S4.

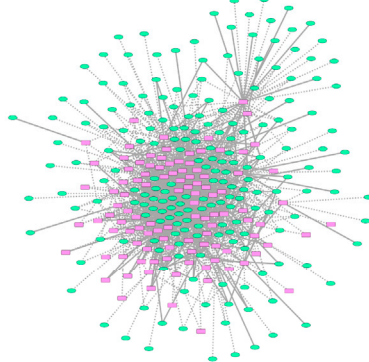


A



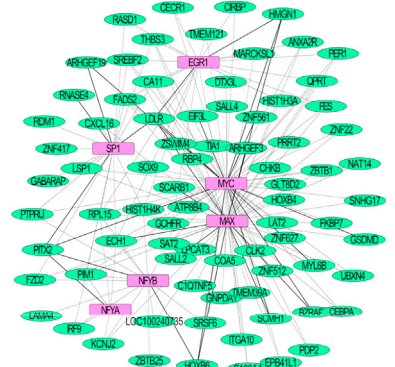
B

Hypermethylated TFBS Network

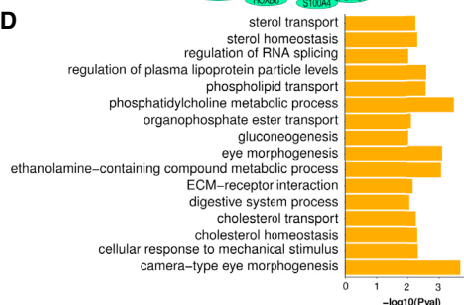


C

MSC master TF network



D



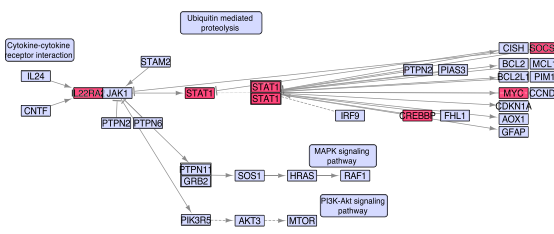
E

	Hyper	Hypo
Wnt signaling pathway	9	0
Viral carcinogenesis	14	11
Tuberculosis	9	10
Transcriptional misregulation in cancer	14	18
TNF signaling pathway	8	9
Thyroid hormone signaling pathway	8	0
T cell receptor signaling pathway	6	0
Small cell lung cancer	5	5
Salmonella infection	0	5
Prostate cancer	5	5
Prolactin signaling pathway	7	8
Pertussis	5	0
Osteoclast differentiation	12	14
Melanogenesis	5	0
Measles	0	8
MAPK signaling pathway	13	13
Jak-STAT signaling pathway	0	9
Influenza A	9	11
Inflammatory bowel disease (IBD)	5	6
Huntington's disease	11	0
HTLV-I infection	22	20
Herpes simplex infection	10	13
Hepatitis C	8	10
Hepatitis B	17	14
Estrogen signaling pathway	6	6
ErbB signaling pathway	5	0
Epstein-Barr virus infection	10	0
Chronic myeloid leukemia	6	6
Cell cycle	7	7
Basal transcription factors	5	0
B cell receptor signaling pathway	5	5
Antigen processing and presentation	5	0
Amphetamine addiction	5	0
Acute myeloid leukemia	6	6

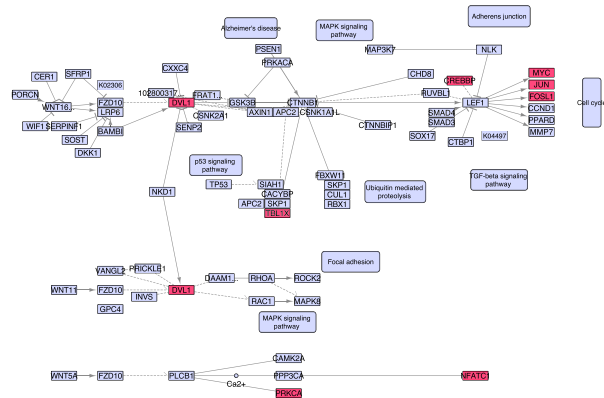
$-\log_{10}(P-value)$ color scale: 0 (white) to 10 (dark red).

F

JAK-STAT signaling pathway



WNT signaling pathway



(legend on next page)



DMCs and DMRs across groups. Hyper- and hypomethylation events at regulatory elements are likely impacting gene expression and cellular function. When these events occur elsewhere in the genome, the impact is less clear, but may not be innocuous. For example, it is feasible that hypo DMRs may lead to increased mutational load through the inability to repair point mutations by the lack of a hemi-methylated strand during replication and repair, or through chromosomal instability, which has been associated with DNA demethylation (Rodriguez et al., 2006). On caveat of our study, and others like it, is that bisulfite conversion does not distinguish between 5mC and 5hmC (hydroxymethylation). A recent study found approximately 1,600 age-associated 5hmC changes in BM-MSCs (Torano et al., 2016). The 5hmC state has not shown to be repressive, and it is likely not to impact TF binding.

A recent study showed that age-associated DNA methylation changes can be reset by reprogramming BM-MSCs followed by redifferentiation to the MSC state, and thereby rejuvenating the MSCs (Frobel et al., 2014). This study was conducted using array-based methods, but future genome-wide assessment of DNA methylation in rejuvenated MSCs should help identify DMCs at regulatory elements that are drivers of age-association BM-MSC decline relative to passenger methylation events. By generating regulatory network and pathway analyses based on more comprehensive epigenomic and TFBS datasets, we provide a better understanding of how the DNA methylome changes with age and alters gene expression and known functionality of human BM-MSCs.

EXPERIMENTAL PROCEDURES

See [Supplemental Experimental Procedures](#) for additional details.

Isolation and Cell Culture of BM-MSCs

Human BM-MSCs from five aged (from 62 to 82 years of age, mean 74.6 years) and five young adult donors (from 20 to 24, mean 22.2 years) were isolated and cultured as described previously following institutional ethical guidelines (Kilpinen et al., 2013; Leskelä et al., 2003; Peura et al., 2009).

ERRBS and WGBS Library Preparation

For ERRBS, DNA (10 ng) was digested with MspI (Thermo Fisher Scientific, catalog no. FD0544) and subjected to bisulfite conversion and Illumina library preparation.

ERRBS and WGBS Data Analysis

Sequencing data were processed to remove adapter matching bases, and poor quality reads or reads with less than 20 bp. Processed reads were mapped to lambda genome and hg19 version of the human genome using Bismark/Bowtie. Bisulfite conversion was assessed using the coverage and methylation status of CpGs mapped on lambda genome. Further methylation calling of CpGs was performed with Bismark (Krueger and Andrews, 2011). Additional methylation analysis involving normalization, overlaps with DHSs, H3K4me1, and ENCODE TFBS data were performed using R/Bioconductor packages.

DMRs Identification

CpG methylation values were smoothed using the BSmooth algorithm (bsseq Bioconductor package) with default parameters and then DMRs were identified (Hansen et al., 2012). We defined a cutoff for the t-statistics (-2.6, +2.6) and further filtered DMRs containing at least three CpGs and showing a mean methylation difference between aged and young donors greater than ± 0.25 (25%).

Significant TFBS Identification

TFBS data were downloaded from ENCODE. Peaks from control experiments were filtered. Data from multiple experiments were reduced to represent a single list of binding sites per TF. TFs not expressed in BM-MSCs were removed, retaining only BM-MSC-expressed TFs for further analyses. DMCs were overlapped with the TFBSs to identify the disrupted TFBS. We used the Fisher's exact test to identify the TFBSs significantly enriched with DMCs. The significant TFBSs are filtered with p values <0.05. The p values are adjusted for multiple hypothesis correction using Benjamini-Hochberg method prior to filtering.

ACCESSION NUMBERS

The raw sequencing data reported in this paper are available from Sequence Read Archive (SRA) using the SRA accession number SRP111740.

Figure 7. Identification of Enriched TFs, Networks, and Pathways

(A) Heatmaps of TFs significantly enriched with DMCs at their binding sites shown as $-\log_{10}$ (adjusted p values) for hyper and hypo conditions.

(B and C) The *in silico* transcriptional regulatory network. (B) Hyper network: the TFs (represented in magenta color) are enriched with hypermethylated CpGs and genes are repressed DEGs (represented in green color). See [Figure S5](#) for the hypo network. (C) The sub-network of significant MSC master regulators (hypermethylated) and their repressed DEGs. Solid lines denote direct target of TFs and dotted lines denote indirect targets.

(D) Gene ontology terms enriched for sub-network.

(E) Heatmap of overrepresented pathways. The numbers indicate the number of TFs and/or DEGs involved in the pathway.

(F) The significantly enriched WNT and JAK-STAT signaling pathways from the hyper and hypo networks, respectively. The TFs and/or DEGs involved in these pathways are highlighted in red. See also [Figures S5](#) and [S6](#), and [Table S7](#).



SUPPLEMENTAL INFORMATION

Supplemental Information includes Supplemental Experimental Procedures, six figures, and seven tables and can be found with this article online at <http://dx.doi.org/10.1016/j.stemcr.2017.07.018>.

AUTHOR CONTRIBUTIONS

K.K.P. performed the methylome experiments, processed and analyzed the sequencing data, and conducted the integrative analysis. N.D.J. contributed to the integrative analysis and DMR analysis and performed the network and pathway analyses. C.A. and S.L.B. contributed to analysis. P.L., L.K., M.K., and S.L. provided the MSCs used in this project. L.K., S.L., and R.L. conceived and designed the MSC study selection. K.K.P., N.D.J., L.K., R.L., S.L., and R.D.H. contributed to data interpretation. K.K.P., N.D.J., L.K., R.L., S.L., and R.D.H. wrote and edited the manuscript.

ACKNOWLEDGMENTS

This project was supported in part by funding from the Academy of Finland (259913), Biocenter Finland, the NIH, the Washington Life Sciences Discovery Fund (265508), and the SalWe Research Program for IMO (Tekes - the Finnish Funding Agency for Technology and Innovation grant 648/10). We acknowledge the Finnish Functional Genomics Center core facility for sequencing services.

Received: November 30, 2016

Revised: July 20, 2017

Accepted: July 21, 2017

Published: August 24, 2017

REFERENCES

Akalin, A., Garrett-Bakelman, F.E., Kormaksson, M., Busuttill, J., Zhang, L., Khrebtkova, I., Milne, T.A., Huang, Y., Biswas, D., Hess, J.L., et al. (2012). Base-pair resolution DNA methylation sequencing reveals profoundly divergent epigenetic landscapes in acute myeloid leukemia. *PLoS Genet.* *8*, e1002781.

Bentivegna, A., Miloso, M., Riva, G., Foudah, D., Butta, V., Dalprà, L., and Tredici, G. (2013). DNA methylation changes during in vitro propagation of human mesenchymal stem cells: implications for their genomic stability? *Stem Cells Int.* *2013*, e192425.

Bhandari, D.R., Seo, K.-W., Jung, J.-W., Kim, H.-S., Yang, S.-R., and Kang, K.-S. (2011). The regulatory role of c-MYC on HDAC2 and PcG expression in human multipotent stem cells. *J. Cell. Mol. Med.* *15*, 1603–1614.

Blattler, A., and Farnham, P.J. (2013). Crosstalk between site-specific transcription factors and DNA methylation states. *J. Biol. Chem.* *288*, 34287–34294.

Blattler, A., Yao, L., Witt, H., Guo, Y., Nicolet, C.M., Berman, B.P., and Farnham, P.J. (2014). Global loss of DNA methylation uncovers intronic enhancers in genes showing expression changes. *Genome Biol.* *15*, 469.

Boks, M.P., Derks, E.M., Weisenberger, D.J., Strengman, E., Janson, E., Sommer, I.E., Kahn, R.S., and Ophoff, R.A. (2009). The relation-

ship of DNA methylation with age, gender and genotype in twins and healthy controls. *PLoS One* *4*, e6767.

Bork, S., Pfister, S., Witt, H., Horn, P., Korn, B., Ho, A.D., and Wagner, W. (2010). DNA methylation pattern changes upon long-term culture and aging of human mesenchymal stromal cells. *Aging Cell* *9*, 54–63.

Brenet, F., Moh, M., Funk, P., Feierstein, E., Viale, A.J., Socci, N.D., and Scandura, J.M. (2011). DNA methylation of the first exon is tightly linked to transcriptional silencing. *PLoS One* *6*, e14524.

Choi, M.R., In, Y.-H., Park, J., Park, T., Jung, K.H., Chai, J.C., Chung, M.K., Lee, Y.S., and Chai, Y.G. (2012). Genome-scale DNA methylation pattern profiling of human bone marrow mesenchymal stem cells in long-term culture. *Exp. Mol. Med.* *44*, 503–512.

ENCODE Project Consortium, Bernstein, B.E., Birney, E., Dunham, L., Green, E.D., Gunter, C., and Snyder, M. (2012). An integrated encyclopedia of DNA elements in the human genome. *Nature* *489*, 57–74.

Fernández, A.F., Bayón, G.F., Urdinguio, R.G., Toraño, E.G., García, M.G., Carella, A., Petrus-Reurer, S., Ferrero, C., Martínez-Cambor, P., Cubillo, I., et al. (2014). H3K4me1 marks DNA regions hypomethylated during aging in human stem and differentiated cells. *Genome Res.* *25*, 27–40.

Frobel, J., Hemeda, H., Lenz, M., Abagnale, G., Jousen, S., Denecke, B., Sarić, T., Zenke, M., and Wagner, W. (2014). Epigenetic rejuvenation of mesenchymal stromal cells derived from induced pluripotent stem cells. *Stem Cell Reports* *3*, 414–422.

Hansen, K., Langmead, B., and Irizarry, R. (2012). BSmooth: from whole genome bisulfite sequencing reads to differentially methylated regions. *Genome Biol.* *13*, R83.

Hänzelmann, S., Beier, F., Gusmao, E.G., Koch, C.M., Hummel, S., Charapitsa, I., Jousen, S., Benes, V., Brümmendorf, T.H., Reid, G., et al. (2015). Replicative senescence is associated with nuclear reorganization and with DNA methylation at specific transcription factor binding sites. *Clin. Epigenetics* *7*, 19.

Heyn, H., Li, N., Ferreira, H.J., Moran, S., Pisano, D.G., Gomez, A., Diez, J., Sanchez-Mut, J.V., Setien, F., Carmona, F.J., et al. (2012). Distinct DNA methylomes of newborns and centenarians. *Proc. Natl. Acad. Sci. USA* *109*, 10522–10527.

Hon, G.C., Rajagopal, N., Shen, Y., McCleary, D.F., Yue, F., Dang, M.D., and Ren, B. (2013). Epigenetic memory at embryonic enhancers identified in DNA methylation maps from adult mouse tissues. *Nat. Genet.* *45*, 1198–1206.

Irizarry, R.A., Ladd-Acosta, C., Wen, B., Wu, Z., Montano, C., Onyango, P., Cui, H., Gabo, K., Rongione, M., Webster, M., et al. (2009). The human colon cancer methylome shows similar hypo- and hypermethylation at conserved tissue-specific CpG island shores. *Nat. Genet.* *41*, 178–186.

Kanfi, Y., Naiman, S., Amir, G., Peshti, V., Zinman, G., Nahum, L., Bar-Joseph, Z., and Cohen, H.Y. (2012). The sirtuin SIRT6 regulates lifespan in male mice. *Nature* *483*, 218–221.

Kilpinen, L., Tigistu-Sahle, F., Oja, S., Greco, D., Parmar, A., Saavalainen, P., Nikkilä, J., Korhonen, M., Lehenkari, P., Käkälä, R., et al. (2013). Aging bone marrow mesenchymal stromal cells have altered membrane glycerophospholipid composition and functionality. *J. Lipid Res.* *54*, 622–635.



- Kim, N., and Cho, S.-G. (2015). New strategies for overcoming limitations of mesenchymal stem cell-based immune modulation. *Int. J. Stem Cells* 8, 54–68.
- Koch, C.M., Jousen, S., Schellenberg, A., Lin, Q., Zenke, M., and Wagner, W. (2012). Monitoring of cellular senescence by DNA-methylation at specific CpG sites. *Aging Cell* 11, 366–369.
- Koch, C.M., Reck, K., Shao, K., Lin, Q., Jousen, S., Ziegler, P., Walenda, G., Drescher, W., Opalka, B., May, T., et al. (2013). Pluripotent stem cells escape from senescence-associated DNA methylation changes. *Genome Res.* 23, 248–259.
- Krueger, F., and Andrews, S.R. (2011). Bismark: a flexible aligner and methylation caller for Bisulfite-Seq applications. *Bioinformatics* 27, 1571–1572.
- L'Episcopo, F., Tirolo, C., Caniglia, S., Testa, N., Morale, M.C., Serapide, M.F., Pluchino, S., and Marchetti, B. (2014). Targeting Wnt signaling at the neuroimmune interface for dopaminergic neuroprotection/repair in Parkinson's disease. *J. Mol. Cell Biol.* 6, 13–26.
- Leskelä, H.-V., Risteli, J., Niskanen, S., Koivunen, J., Ivaska, K.K., and Lehenkari, P. (2003). Osteoblast recruitment from stem cells does not decrease by age at late adulthood. *Biochem. Biophys. Res. Commun.* 311, 1008–1013.
- Leucht, P., Kim, J.-B., Amasha, R., James, A.W., Girod, S., and Helms, J.A. (2008). Embryonic origin and Hox status determine progenitor cell fate during adult bone regeneration. *Development* 135, 2845–2854.
- Lister, R., Pelizzola, M., Dowen, R.H., Hawkins, R.D., Hon, G., Tonti-Filippini, J., Nery, J.R., Lee, L., Ye, Z., Ngo, Q.-M., et al. (2009). Human DNA methylomes at base resolution show widespread epigenomic differences. *Nature* 462, 315–322.
- McClay, J.L., Aberg, K.A., Clark, S.L., Nerella, S., Kumar, G., Xie, L.Y., Hudson, A.D., Harada, A., Hultman, C.M., Magnusson, P.K.E., et al. (2014). A methylome-wide study of aging using massively parallel sequencing of the methyl-CpG-enriched genomic fraction from blood in over 700 subjects. *Hum. Mol. Genet.* 23, 1175–1185.
- Müller, F.-J., Laurent, L.C., Kostka, D., Ulitsky, I., Williams, R., Lu, C., Park, I.-H., Rao, M.S., Shamir, R., Schwartz, P.H., et al. (2008). Regulatory networks define phenotypic classes of human stem cell lines. *Nature* 455, 401–405.
- Nalapareddy, K., Nattamai, K.J., Kumar, R.S., Karns, R., Wikenheiser-Brokamp, K.A., Sampson, L.L., Mahe, M.M., Sundaram, N., Yacyshyn, M.-B., Yacyshyn, B., et al. (2017). Canonical Wnt signaling ameliorates aging of intestinal stem cells. *Cell Rep.* 18, 2608–2621.
- Peura, M., Bizik, J., Salmenperä, P., Noro, A., Korhonen, M., Pätilä, T., Vento, A., Vaheri, A., Alitalo, R., Vuola, J., et al. (2009). Bone marrow mesenchymal stem cells undergo neosis and induce keratinocyte wound healing utilizing the HGF/c-Met/PI3K pathway. *Wound Repair Regen.* 17, 569–577.
- Phinney, D.G., and Prockop, D.J. (2007). Concise review: mesenchymal stem/multipotent stromal cells: the state of transdifferentiation and modes of tissue repair—current views. *Stem Cells* 25, 2896–2902.
- Price, F.D., von Maltzahn, J., Bentzinger, C.F., Dumont, N.A., Yin, H., Chang, N.C., Wilson, D.H., Frenette, J., and Rudnicki, M.A. (2014). Inhibition of JAK-STAT signaling stimulates adult satellite cell function. *Nat. Med.* 20, 1174–1181.
- Prokhortchouk, A., Hendrich, B., Jørgensen, H., Ruzov, A., Wilm, M., Georgiev, G., Bird, A., and Prokhortchouk, E. (2001). The p120 catenin partner Kaiso is a DNA methylation-dependent transcriptional repressor. *Genes Dev.* 15, 1613–1618.
- Roadmap Epigenomics Consortium, Kundaje, A., Meuleman, W., Ernst, J., Bilenky, M., Yen, A., Heravi-Moussavi, A., Kheradpour, P., Zhang, Z., Wang, J., et al. (2015). Integrative analysis of 111 reference human epigenomes. *Nature* 518, 317–330.
- Rodriguez, J., Frigola, J., Vendrell, E., Risques, R.-A., Fraga, M.F., Morales, C., Moreno, V., Esteller, M., Capellà, G., Ribas, M., et al. (2006). Chromosomal instability correlates with genome-wide DNA demethylation in human primary colorectal cancers. *Cancer Res.* 66, 8462–9468.
- Roson-Burgo, B., Sanchez-Guijo, F., Del Cañizo, C., and De Las Rivas, J. (2014). Transcriptomic portrait of human mesenchymal stromal/stem cells isolated from bone marrow and placenta. *BMC Genomics* 15, 910.
- Ruiz de Eguino, G., Infante, A., Schlangen, K., Aransay, A.M., Fullaondo, A., Soriano, M., García-Verdugo, J.M., Martín, A.G., and Rodríguez, C.I. (2012). Sp1 transcription factor interaction with accumulated prelamin A impairs adipose lineage differentiation in human mesenchymal stem cells: essential role of sp1 in the integrity of lipid vesicles. *Stem Cells Transl. Med.* 1, 309–321.
- Sandoval, J., Heyn, H., Moran, S., Serra-Musach, J., Pujana, M.A., Bibikova, M., and Esteller, M. (2011). Validation of a DNA methylation microarray for 450,000 CpG sites in the human genome. *Epigenetics* 6, 692–702.
- Schellenberg, A., Lin, Q., Schüler, H., Koch, C.M., Jousen, S., De-neck, B., Walenda, G., Pallua, N., Suschek, C.V., Zenke, M., et al. (2011). Replicative senescence of mesenchymal stem cells causes DNA-methylation changes which correlate with repressive histone marks. *Aging* 3, 873–888.
- Sheffield, N.C., Thurman, R.E., Song, L., Safi, A., Stamatoyannopoulos, J.A., Lenhard, B., Crawford, G.E., and Furey, T.S. (2013). Patterns of regulatory activity across diverse human cell types predict tissue identity, transcription factor binding, and long-range interactions. *Genome Res.* 23, 777–788.
- Stadler, M.B., Murr, R., Burger, L., Ivanek, R., Lienert, F., Schöler, A., van Nimwegen, E., Wirbelauer, C., Oakeley, E.J., Gaidatzis, D., et al. (2011). DNA-binding factors shape the mouse methylome at distal regulatory regions. *Nature* 480, 490–495.
- Stergachis, A.B., Haugen, E., Shafer, A., Fu, W., Vernot, B., Reynolds, A., Raubitschek, A., Ziegler, S., LeProust, E.M., Akey, J.M., et al. (2013). Exonic transcription factor binding directs codon choice and affects protein evolution. *Science* 342, 1367–1372.
- Thurman, R.E., Rynes, E., Humbert, R., Vierstra, J., Maurano, M.T., Haugen, E., Sheffield, N.C., Stergachis, A.B., Wang, H., Vernot, B., et al. (2012). The accessible chromatin landscape of the human genome. *Nature* 489, 75–82.
- Tierney, M.T., Aydogdu, T., Sala, D., Malecova, B., Gatto, S., Puri, P.L., Latella, L., and Sacco, A. (2014). STAT3 signaling controls satellite cell expansion and skeletal muscle repair. *Nat. Med.* 20, 1182–1186.



Toraño, E.G., Bayón, G.F., Del Real, Á., Sierra, M.I., García, M.G., Carella, A., Belmonte, T., Urduño, R.G., Cubillo, I., García-Castro, J., et al. (2016). Age-associated hydroxymethylation in human bone-marrow mesenchymal stem cells. *J. Transl. Med.* *14*, 207.

Wagner, J.R., Busche, S., Ge, B., Kwan, T., Pastinen, T., and Blanche, M. (2014). The relationship between DNA methylation, genetic and expression inter-individual variation in untransformed human fibroblasts. *Genome Biol.* *15*, R37.

Wagner, W., Ho, A.D., and Zenke, M. (2010a). Different facets of aging in human mesenchymal stem cells. *Tissue Eng. Part B Rev.* *16*, 445–453.

Wagner, W., Bork, S., Lepperdinger, G., Jousen, S., Ma, N., Strunk, D., and Koch, C. (2010b). How to track cellular aging of mesenchymal stromal cells? *Aging* *2*, 224–230.

Yi, T., Lee, D.-S., Jeon, M.-S., Kwon, S.W., and Song, S.U. (2012). Gene expression profile reveals that STAT2 is involved in the immunosuppressive function of human bone marrow-derived mesenchymal stem cells. *Gene* *497*, 131–139.

Zhu, J., Zhang, Y., Joe, G.J., Pompetti, R., and Emerson, S.G. (2005). NF- κ B activates multiple hematopoietic stem cell (HSC) regulatory genes and promotes HSC self-renewal. *Proc. Natl. Acad. Sci. USA* *102*, 11728–11733.

Stem Cell Reports, Volume 9

Supplemental Information

**Methylome Analysis of Human Bone Marrow MSCs Reveals Extensive
Age- and Culture-Induced Changes at Distal Regulatory Elements**

Kalyan K. Pasumathy, Naresh Doni Jayavelu, Lotta Kilpinen, Colin Andrus, Stephanie L. Battle, Matti Korhonen, Petri Lehenkari, Riikka Lund, Saara Laitinen, and R. David Hawkins

Figure S1

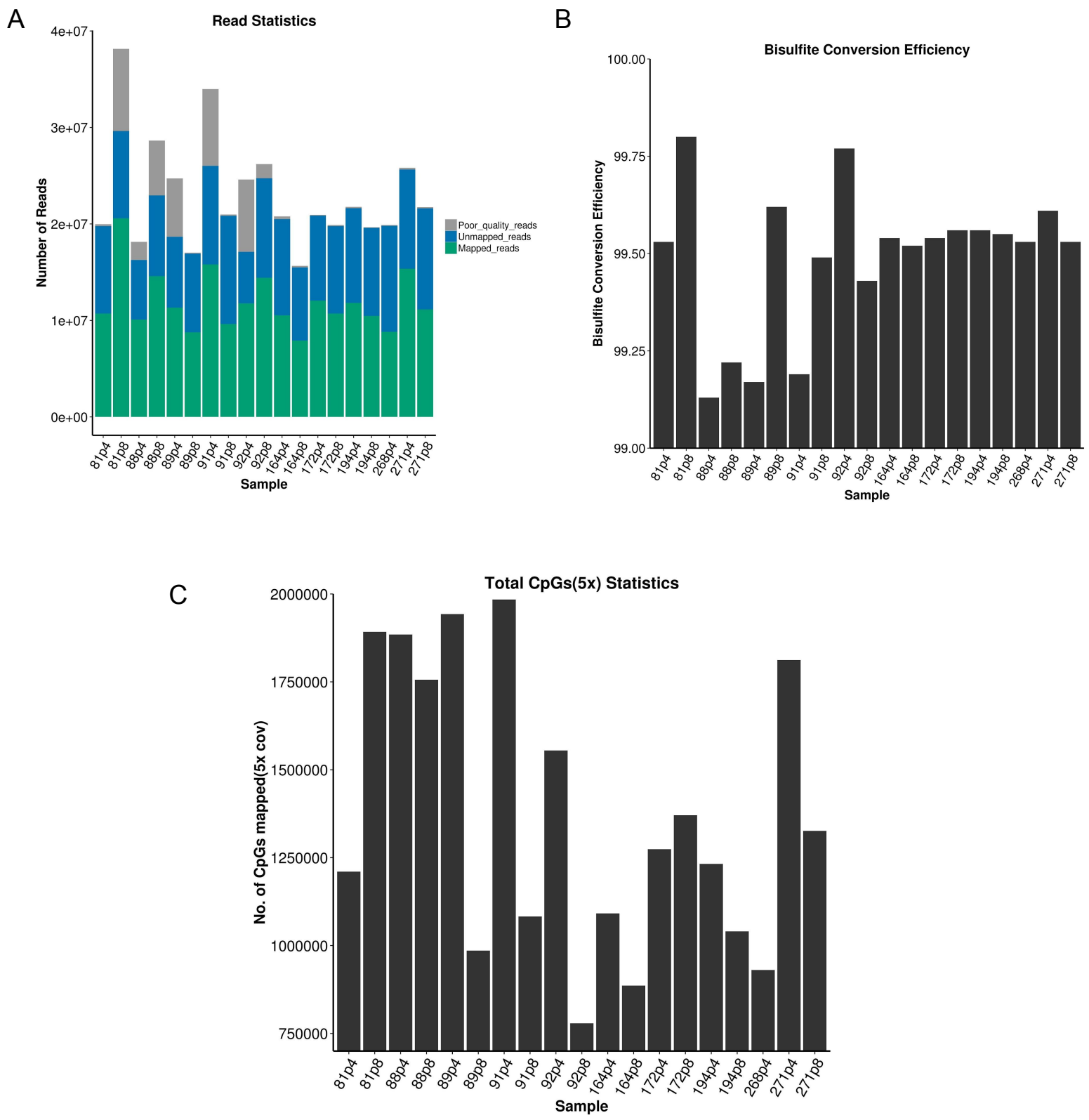


Figure S1. Enhanced RRBS stats. A) Methylation across the genome was captured using ERRBS (Illumina 1 x 50 bp single end sequencing). Around 50-60% of the reads were mapped to the hg19 version of the human genome. B) The data were examined for the efficiency of bisulfite conversion and is > 99% in all samples. C) Reads were mapped to hg19 and total CpGs were assessed. Number of CpGs captured varied from sample to sample and are in the range of 750,000 - 2,000,000. Related Figure 1.

Figure S2

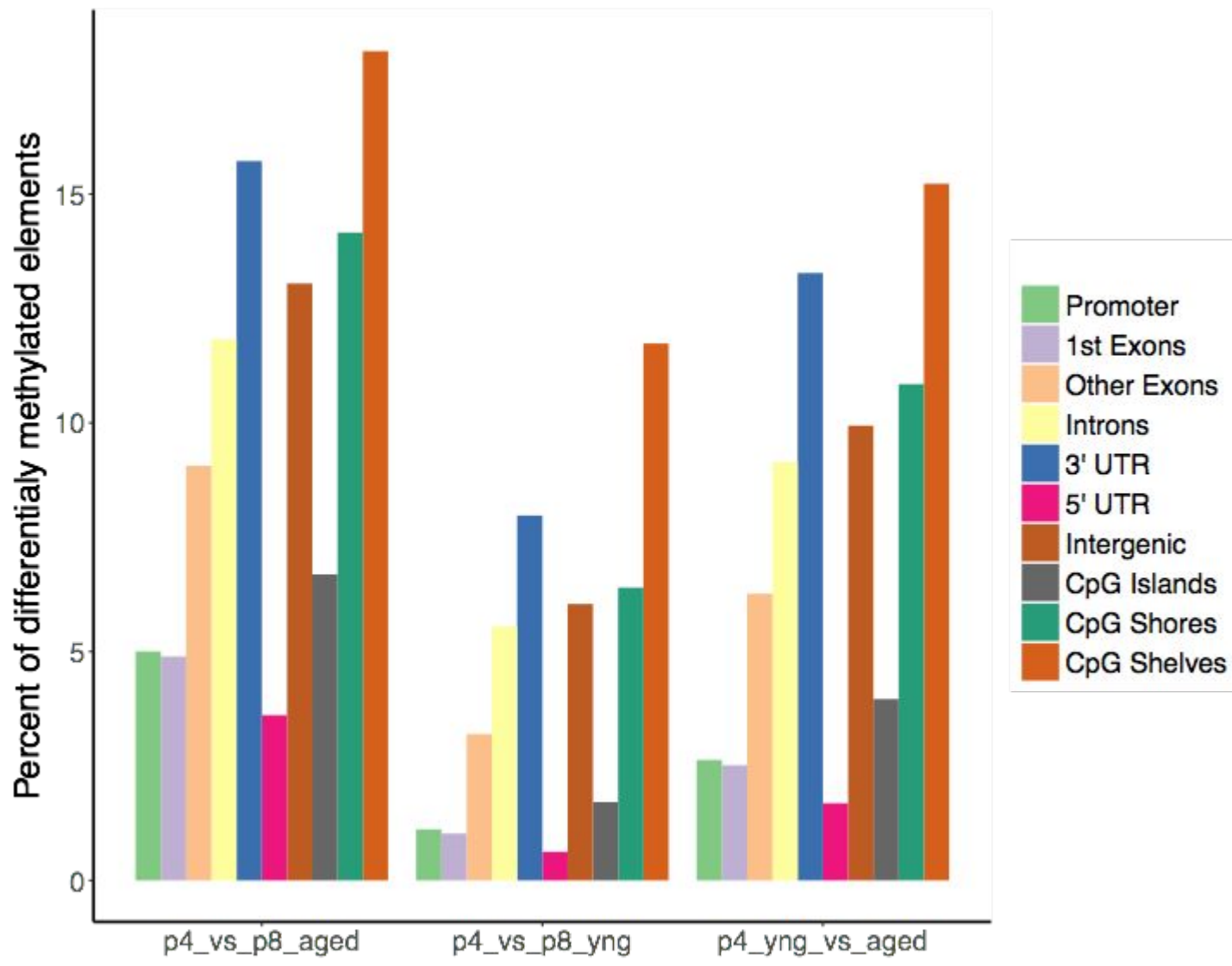


Figure S2. Percent of Genic and CpG annotated Elements with Differential Methylation. For each comparison (culture effect in aged - left; culture effect in young - center; age-associated - right) of ERRBS data, the percent of mapped elements that overlap at least one DMC are shown from left to right: promoters, 1st exons, all other exons, introns, 3' UTRs, 5' UTRs, intergenic regions, CpG islands, CG island shores, and CG island shelves. Related to Figure 2.

Figure S3

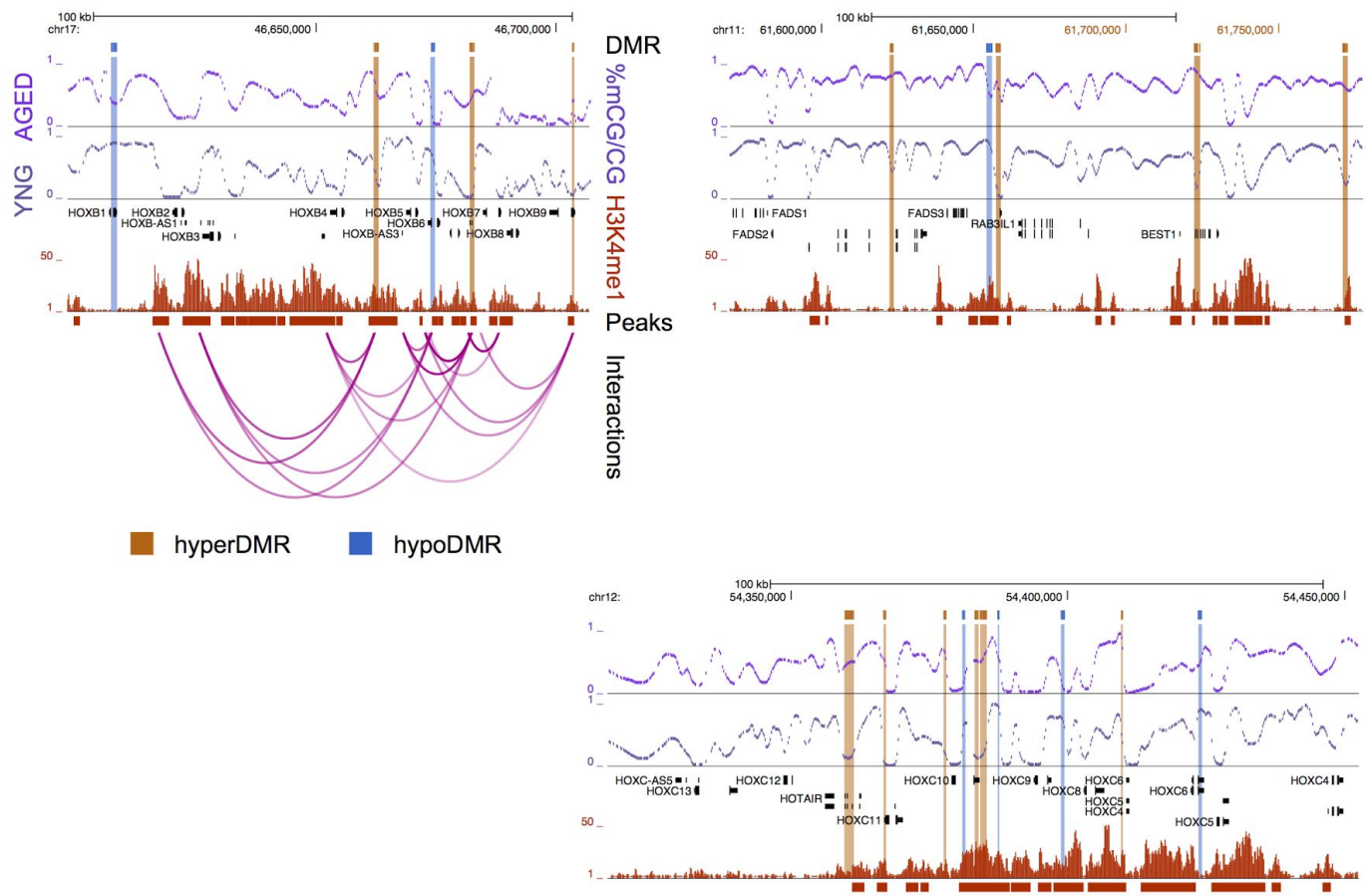


Figure S3. Browser shots of *HOXB*, *HOXC* and *FADS* gene cluster. This figure is as described in Figure 5 in the main text, and highlights DMRs at enhancer elements within the *HOXB*, *HOXC* and *FADS* gene clusters, which contains several genes down-regulated with age. Related to Figure 5.

Figure S4

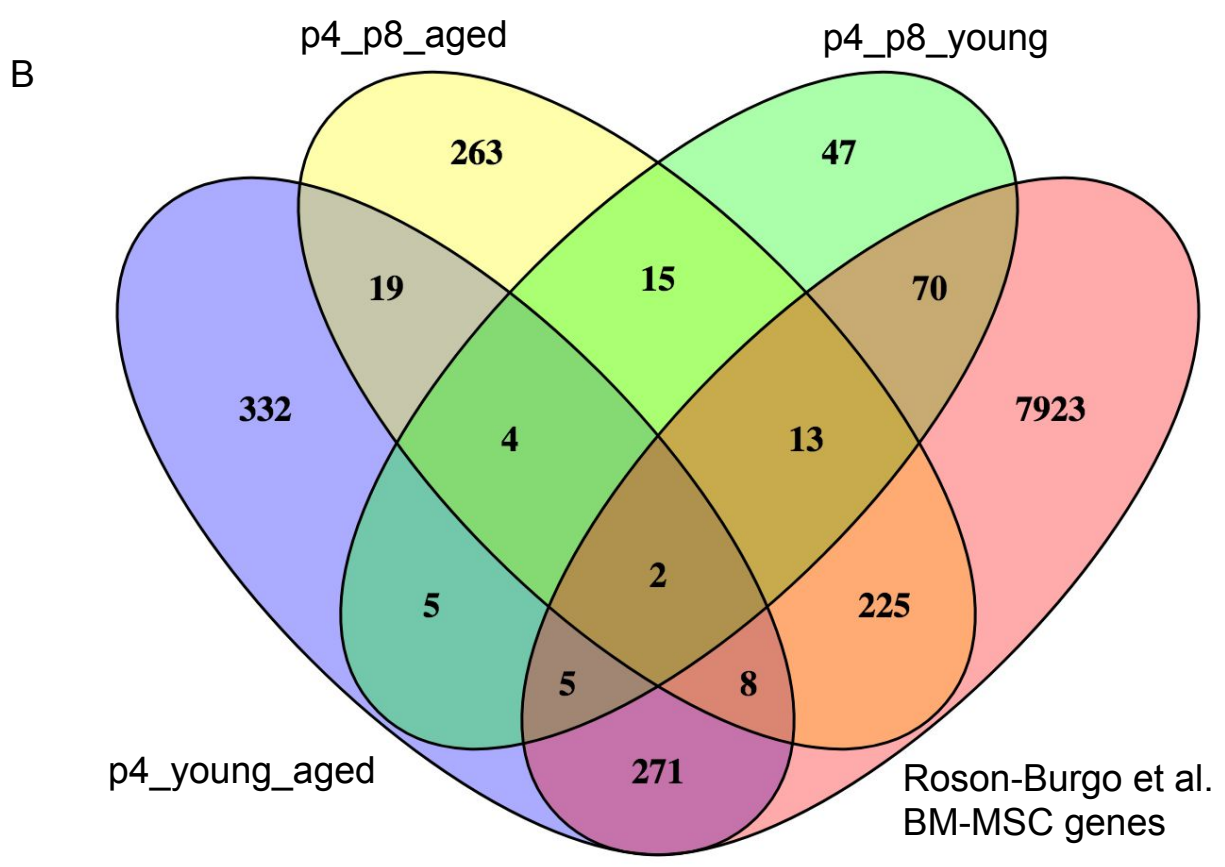
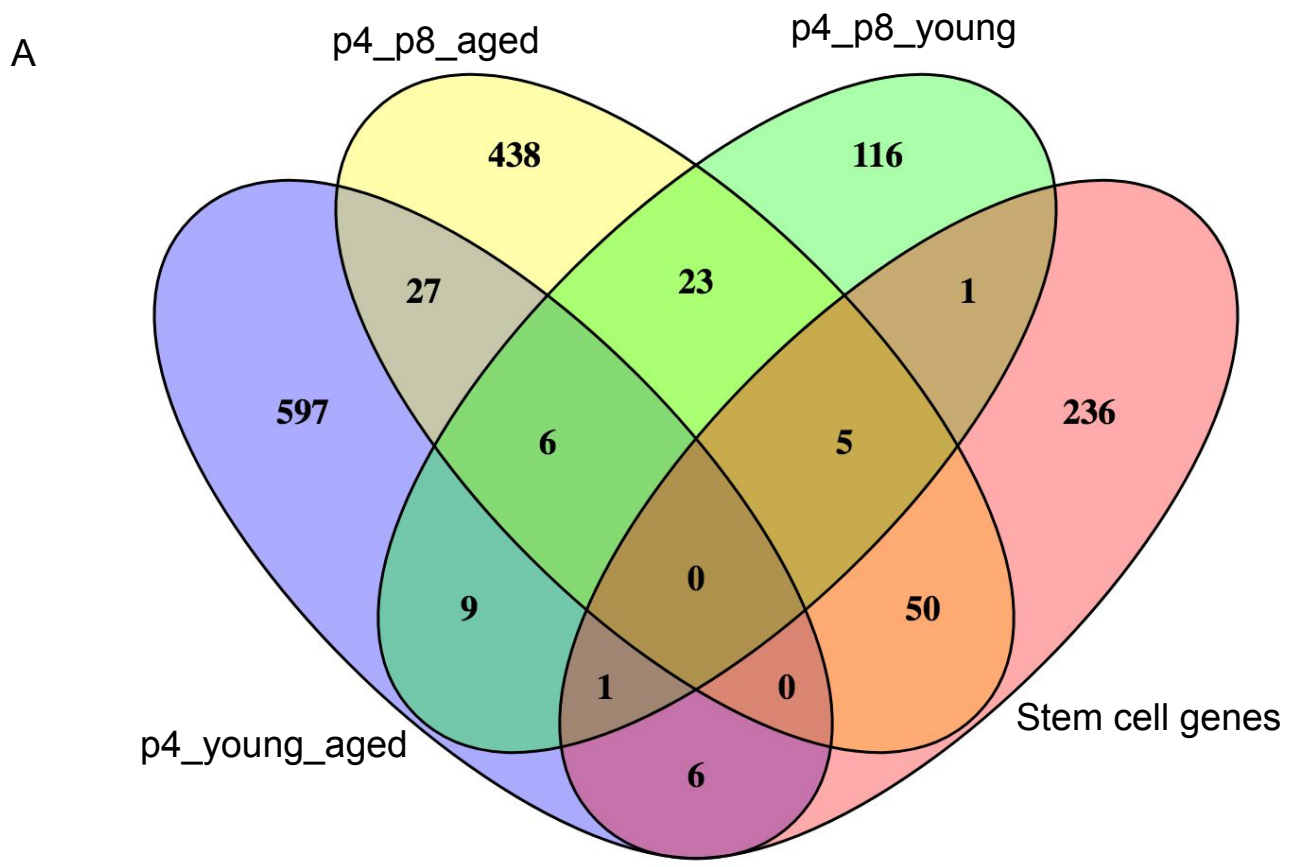


Figure S4. Overlap of BM-MS genes. Overlap of BM-MS genes from this study with stem cell genes from Muller et al., 2008 (A) and BM-MS genes from Roson-Burgo et al., 2014 (B) comparisons. Related to Figure 6.

Figure S5

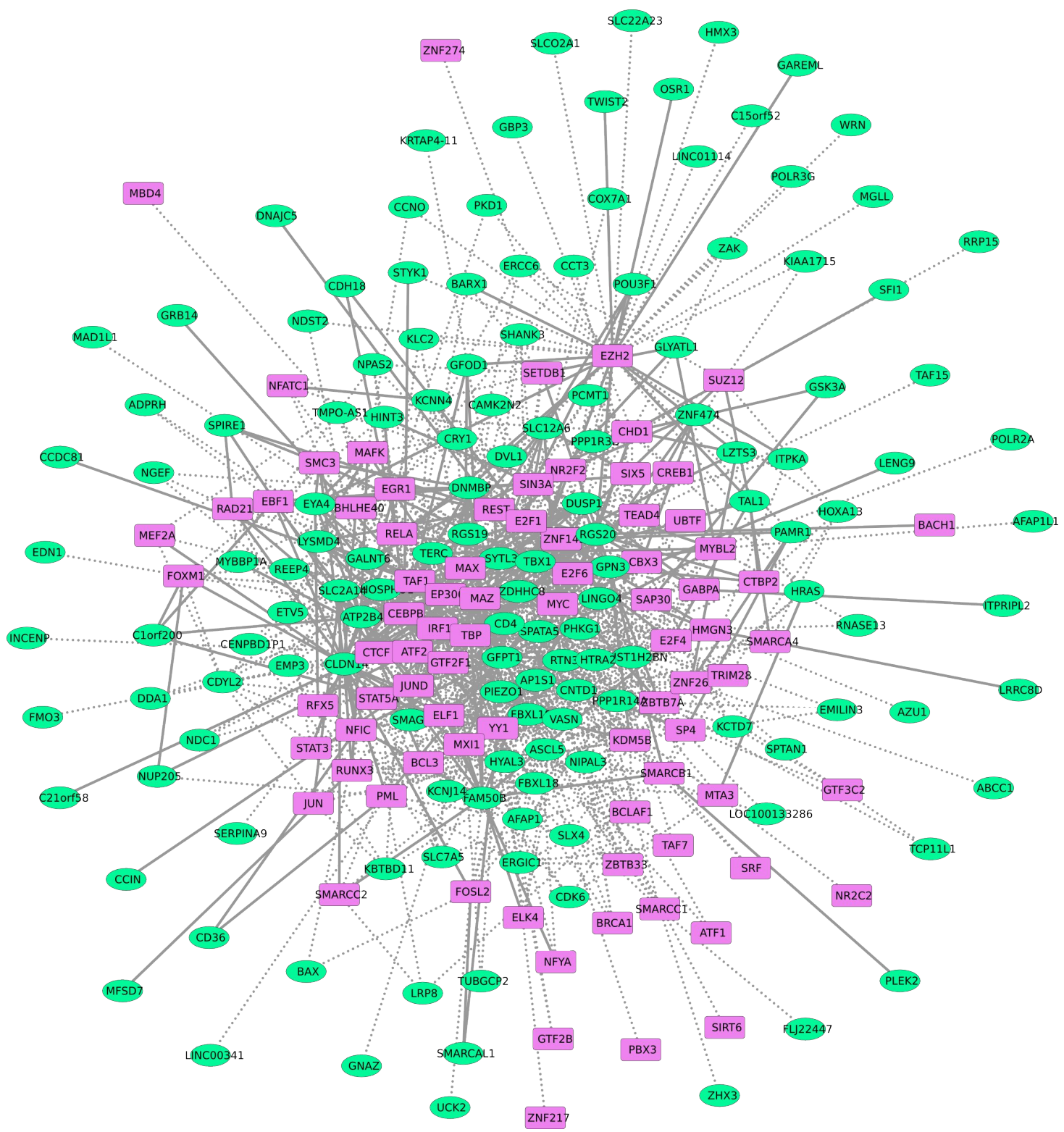


Figure S5. The *in silico* Hypomethylation Transcriptional Regulatory Network. The TFs (represented in magenta color) are enriched with hypomethylated CpGs and genes are activated DEGs (represented in green color), or increase with age. Here, solid lines denote direct target of TFs and dotted lines denote indirect targets. Related to Figure 7.

Figure S6

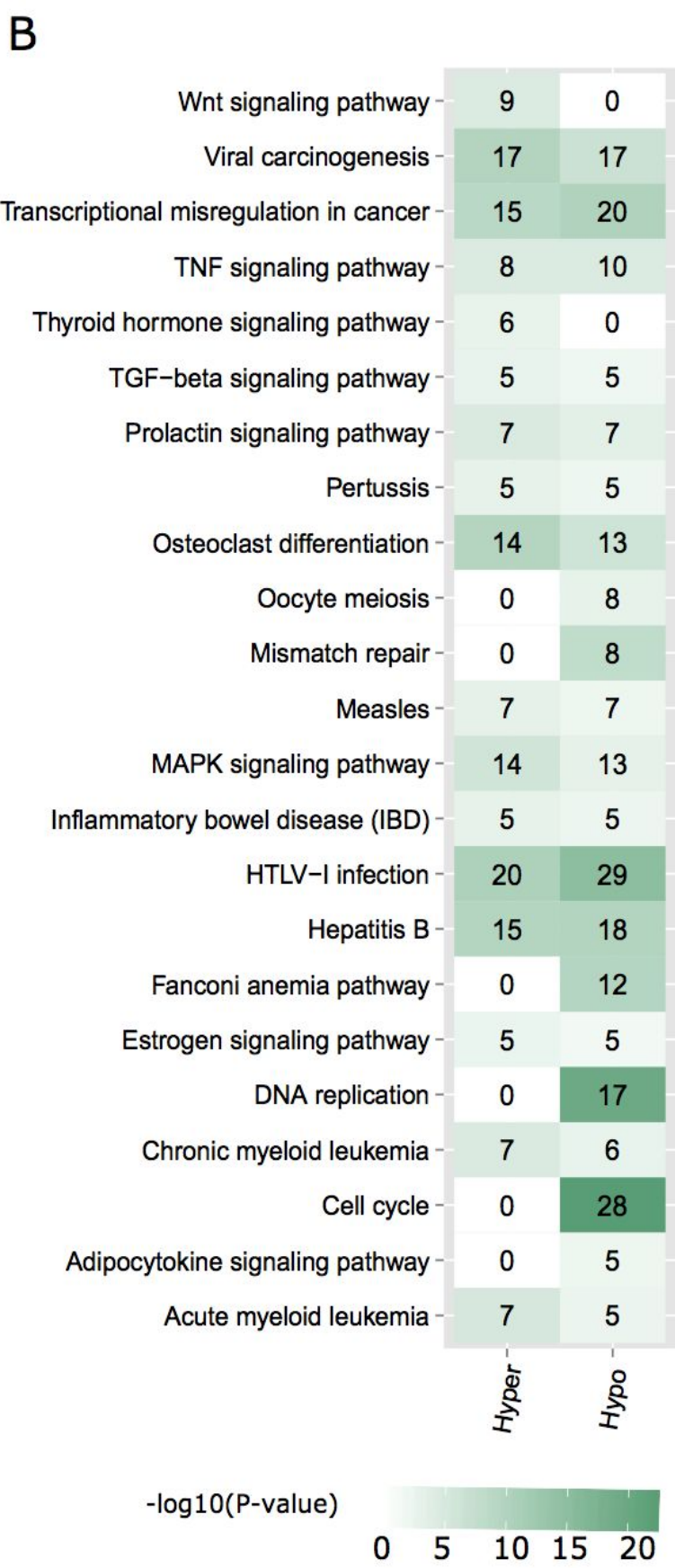
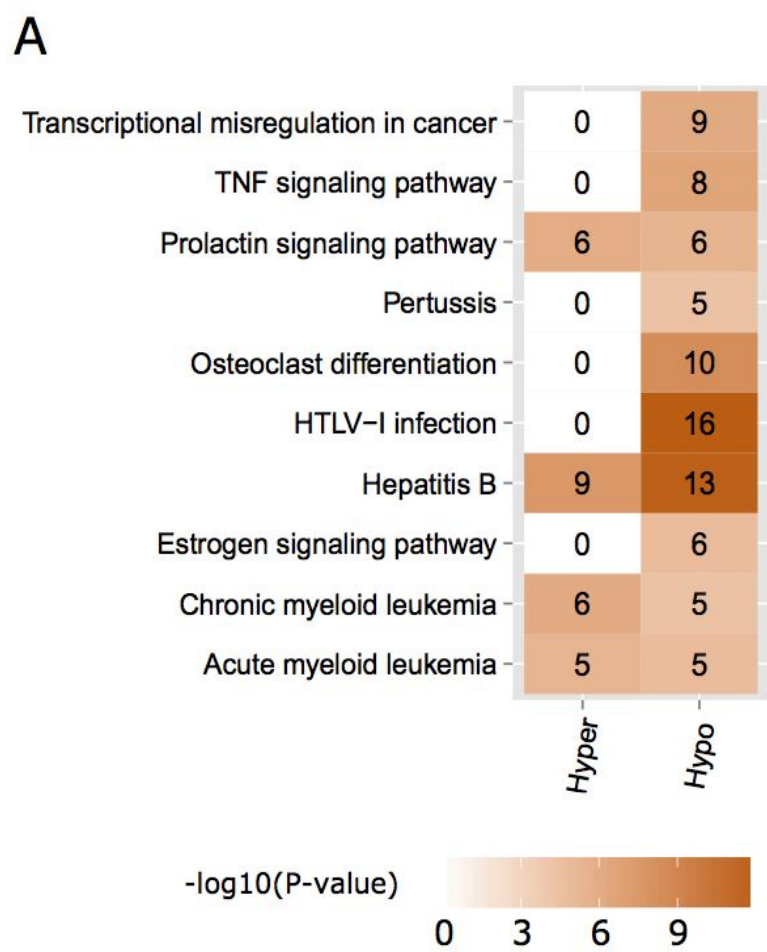


Figure S6. Overrepresented Pathways for Culture Induced Changes. Overrepresented pathways are identified with the list of transcription factors and differentially expressed genes (DEGs) from the p4_vs_p8_yng (A) and p4_vs_p8_aged (B) comparisons. The numbers indicate the number of TFs and/or DEGs involved in the pathway. Related to Figure 7.

Table 1.1

	Number (Percent) of CpGs mapped to genic elements					
File_name	Promoters	First Exons	Other exons	Introns	3' UTRs	5' UTRs
p4_vs_p8_aged	108097 (17%)	88329 (13.89%)	65514 (10.3%)	254317 (40%)	10597 (1.67%)	55061 (8.66%)
p4_vs_p8_yng	108476 (21.94%)	91837 (18.58%)	38650 (7.82%)	187858 (38%)	6571 (1.33%)	57593 (11.65%)
p4_yng_vs_aged	105402 (18.24%)	88712 (15.35%)	53699 (9.29%)	228591 (39.56%)	9017 (1.56%)	55004 (9.52%)

Table 1.2

	Number (Percent) of DMCs mapped to genic elements					
File_name	Promoters	First Exons	Other exons	Introns	3' UTRs	5' UTRs
p4_vs_p8_aged	5409 (6.78%)	4323 (5.42%)	9617 (12.05%)	30085 (37.7%)	1666 (2.09%)	1988 (2.49%)
p4_vs_p8_yng	1210 (4.32%)	941 (3.36%)	3233 (11.54%)	10420 (37.2%)	524 (1.87%)	359 (1.28%)
p4_yng_vs_aged	2774 (5.07%)	2232 (4.08%)	6690 (12.22%)	20896 (38.17%)	1197 (2.19%)	927 (1.69%)

Table 1.3

	Number (Percent) of genic elements mapped with CpGs					
File_name	Promoters	First Exons	Other exons	Introns	3' UTRs	5' UTRs
p4_vs_p8_aged	13917(48.63%)	11929(39.92%)	15260 (7.85%)	45861 (22.17%)	2608 (11.97%)	9,738 (26.28%)
p4_vs_p8_yng	13578 (48.63%)	11927 (39.91%)	10328 (5.32%)	33880 (16.38%)	1810 (8.31%)	9805 (26.46%)
p4_yng_vs_aged	13838 (48.63%)	11866 (39.71%)	13979 (7.19%)	42859 (20.72%)	2431 (11.61%)	9749 (26.31%)

Table 1.4

	Number (Percent) of genic elements mapped with DMCs					
File_name	Promoters	First Exons	Other exons	Introns	3' UTRs	5' UTRs
p4_vs_p8_aged	4662 (16.29%)	3183 (10.65%)	6727 (3.46%)	21721 (10.5%)	1256 (5.76%)	1787 (4.82%)
p4_vs_p8_yng	1076 (3.76%)	720 (2.41%)	2522 (1.3%)	8425 (4.07%)	456 (2.09%)	312 (0.84%)
p4_yng_vs_aged	2188 (7.64%)	1502 (5.03%)	4504 (2.32%)	14822 (7.17%)	875 (4.02%)	786 (2.12%)

Table 2.1

Number (Percent) of CpGs mapped to CpG annotation elements				
File_name	Islands	Shores	Shelves	Outside
p4_vs_p8_aged	290641 (45.72%)	88934 (13.99%)	26623 (4.19%)	229558 (36.11%)
p4_vs_p8_yng	285771 (57.80%)	63889 (12.92%)	14342 (2.90%)	130391 (26.37%)
p4_yng_vs_aged	280207 (48.50%)	78138 (13.52%)	21836 (3.78%)	197588 (3.78%)

Table 2.2

Number (Percent) of DMCs mapped to CpG annotation elements				
File_name	Islands	Shores	Shelves	Outside
p4_vs_p8_aged	19435 (24.36%)	12592 (15.78%)	4825 (6.05%)	42944 (53.82%)
p4_vs_p8_yng	4891 (17.46%)	4088 (14.59%)	1683 (6.01%)	17351 (61.94%)
p4_yng_vs_aged	11107 (20.29%)	8475 (15.48%)	3325 (6.07%)	31843 (58.16%)

Table 2.3

Number (Percent) of CpG annotation elements mapped with all CpGs			
File_name	Islands	Shores	Shelves
p4_vs_p8_aged	19169 (71.95%)	19885 (41.25%)	7388 (18.19%)
p4_vs_p8_yng	18265 (68.56%)	16645 (34.53%)	4796 (11.81%)
p4_yng_vs_aged	18864 (70.81%)	19006 (39.42%)	6663 (16.4%)

Table 2.4

Number (Percent) of CpG annotation elements mapped with DMCs			
File_name	Islands	Shores	Shelves
p4_vs_p8_aged	10670 (55.66%)	9015 (45.34%)	3520 (47.64%)
p4_vs_p8_yng	3033 (16.61%)	3239 (19.46%)	1355 (28.25%)
p4_yng_vs_aged	5397 (28.61%)	5899 (31.04%)	2479 (37.21%)

Table S2. DNA methylation statistics across CpG annotation elements. Related to Figure 2.

Table 5.1

File_name	Number (Percent) of DMCs mapped to genic elements					
	Promoters	First Exons	Other exons	Introns	3' UTRs	5' UTRs
all_early_vs_late	577 (3.98%)	400 (2.76%)	1433 (9.90%)	4973 (34.34%)	249 (1.72%)	164(1.13%)

Table 5.2

Distribution of DMCs across CpG annotation elements during expansion				
File_name	Islands	Shores	Shelves	Outside
all_early_vs_late	2593 (17.9%)	2242 (15.4%)	877(6.05%)	8770 (60.55%)

Table 5.3

File_name	Total DMCs
p4_vs_p8_aged	79796
p4_vs_p8_yng	28013
p4_yng_vs_aged	54750
all_early_vs_late	14482

Table S5. DNA methylation statistics for culture changes irrespective of age.

As excel files:

Table S3. Statistical significance of DMC overlap analysis. Related to Figure 2.

Table S4. Methylation changes at TFBS (ERRBS). Related to Figure 3.

Table S6. Putative enhancer DMR-gene interactions. Related to Figure 5.

Table S7. Biological aging induced DNA methylation changes at TFBS (WGBS). Related to Figure 7.

Supplemental Experimental Procedures

Isolation and Cell Culture of BM-MSCs

Human BM-MSCs were obtained from bone marrow aspirates taken from the iliac crest or upper femur metaphysis of adult patients after written informed consent. All patient protocols were approved by the Ethical Committee of Northern Ostrobothnia Hospital District or Ethical Committee of Hospital District of Helsinki and Uusimaa. Human BM-MSCs from five aged (from 62 to 82 years of age, mean 74.6 years) and five young adult donors (from 20 to 24, mean 22.2 years) were isolated and cultured as previously described (Leskelä et al. 2003; Peura et al. 2009; Kilpinen et al. 2013). Briefly, by growth in minimum essential alpha-medium (α MEM) supplemented with 20mM HEPES, 10% heat inactivated fetal bovine serum (FBS), 2mM L-glutamine and 100 units/mL penicillin and 100 μ g/mL streptomycin (all from Gibco, Invitrogen, Paisley, UK). The same serum lot was used throughout the study. The cells were plated at a density of 1000 cells/cm², medium was renewed twice a week and the cells were harvested when 70-80% confluent. Only four of five aged samples were carried to passage 8 and therefore used in the aged p4_vs_p8 comparison (Figure 1).

ERRBS and WGBS Library Preparation

For ERRBS, DNA (10 ng) was digested with MspI (Thermo Fisher, Cat # FD0544). Digested DNA was subjected to end repair using NEBNext End repair module (New England Biolabs, Cat# E6050S) followed by clean-up with Ampure XP beads. Further subjected to A-tailing reaction using NEBNext-dA-tailing module (Cat# E6053) and clean-up with beads. Purified A-tailed unmethylated lambda DNA (Promega, Cat# D1521) was spiked-in at 0.1-0.5% and mixed with methylated oligo adapters (20 μ M). Ligation was performed with NEBNext Quick Ligation module (New England Biolabs, Cat# E6056S). Ligated DNA was purified with Ampure XP beads. Ligated and purified DNA was subjected to bisulfite conversion using MethylCode Bisulfite conversion kit (Thermo Fisher, Cat# MECOV-50) and purified as per protocol. Purified DNA was subjected to 18 cycles of PCR amplification with KAPA HiFi HotStart Uracil+ (KAPABiosystems Cat# KK2802) and purified. 1-2 μ l of purified library subjected to second round of PCR amplification for 2-4 cycles of PCR and purified with Ampure XP beads. Purified library was subjected to sequencing with Illumina HiSeq 2500 single end 50bp sequencing. For WGBS, genomic DNA (30ng in a

volume of 130 ul) was subjected to sonication using Covaris sonicator until DNA is sheared into fragments of size 40bp to 600bp. Sheared DNA was purified using Ampure XP beads. WGBS libraries were prepared similar to ERRBS library.

ChIP-seq Data Analysis

H3K4me1 data from four human BM-MSC donors was obtained from the Roadmap Epigenome Consortium. Peaks were called using MACS version 1.4.2 on individual H3K4me1 ChIP-seq replicates normalized to input to assess reproducibility (Zhang et al. 2008). Peaks were recalled on merged replicates and used for further analysis.

Gene Expression

Gene expression data from donor samples at each passage was previously described (Kilpinen et al. 2013). Data from this publication were utilized in this work to assess the correlation between gene expression and the methylation changes on the genome.

Pathway Analysis

ClueGO (Bindea et al. 2009) was used to identify the enriched pathways with the data from KEGG pathways. The statistically significant pathways were filtered with P-value < 0.05 and P-values are adjusted with Benjamini Hochberg method for multiple hypothesis correction.

Transcriptional Regulatory Network Construction

First we identified the TFs at significantly enriched with DMCs. Next, we checked whether their TFBS are overlapping within promoter regions of DEGs and termed these DEGs as direct targets. Next, we identified the nearest neighboring gene (NNG) for these TFBS and termed as their indirect targets. In addition, we included only only down- and up-regulated DEGs for hyper and hypomethylated TFs as targets respectively. Cytoscape software (Shannon et al. 2003) was used for visualization of the networks.

DMR-Gene Interaction Data

We downloaded the DHS elements and promoter interaction data from (Sheffield et al. 2013). These interactions are based on correlation between DHS signal intensity and gene expression pattern across numerous human cell types. Only positive correlation interactions are included for further analysis. We overlapped identified DMRs with DHS elements to find DMR-gene interactions further filtered interactions with only differentially expressed genes (DEGs).

SUPPLEMENTARY REFERENCES

- Bindea, Gabriela, Bernhard Mlecnik, Hubert Hackl, Pornpimol Charoentong, Marie Tosolini, Amos Kirilovsky, Wolf-Herman Fridman, Franck Pagès, Zlatko Trajanoski, and Jérôme Galon. 2009. "ClueGO: A Cytoscape Plug-in to Decipher Functionally Grouped Gene Ontology and Pathway Annotation Networks." *Bioinformatics* 25 (8): 1091–93.
- Kilpinen, Lotta, Feven Tigistu-Sahle, Sofia Oja, Dario Greco, Amarjit Parmar, Päivi Saavalainen, Janne Nikkilä, et al. 2013. "Aging Bone Marrow Mesenchymal Stromal Cells Have Altered Membrane Glycerophospholipid Composition and Functionality." *Journal of Lipid Research* 54 (3): 622–35.
- Leskelä, Hannu-Ville, Juha Risteli, Salla Niskanen, Jussi Koivunen, Kaisa K. Ivaska, and Petri Lehenkari. 2003. "Osteoblast Recruitment from Stem Cells Does Not Decrease by Age at Late Adulthood." *Biochemical and Biophysical Research Communications* 311 (4): 1008–13.
- Peura, Matti, Jozef Bizik, Pertteli Salmenperä, Ariel Noro, Matti Korhonen, Tommi Pätilä, Antti Vento, et al. 2009. "Bone Marrow Mesenchymal Stem Cells Undergo Nemo-sis and Induce Keratinocyte Wound Healing Utilizing the HGF/c-Met/PI3K Pathway." *Wound Repair and Regeneration: Official Publication of the Wound Healing Society [and] the European Tissue Repair Society* 17 (4): 569–77.
- Shannon, Paul, Andrew Markiel, Owen Ozier, Nitin S. Baliga, Jonathan T. Wang, Daniel Ramage, Nada Amin, Benno Schwikowski, and Trey Ideker. 2003. "Cytoscape: A Software Environment for Integrated Models of Biomolecular Interaction Networks." *Genome Research* 13 (11): 2498–2504.
- Sheffield, Nathan C., Robert E. Thurman, Lingyun Song, Alexias Safi, John A. Stamatoyannopoulos, Boris Lenhard, Gregory E. Crawford, and Terrence S. Furey. 2013. "Patterns of Regulatory Activity across Diverse Human Cell Types Predict Tissue Identity, Transcription Factor Binding, and Long-Range Interactions." *Genome Research* 23 (5): 777–88.
- Zhang, Yong, Tao Liu, Clifford A. Meyer, Jérôme Eeckhoute, David S. Johnson, Bradley E. Bernstein, Chad Nusbaum, et al. 2008. "Model-Based Analysis of ChIP-Seq (MACS)." *Genome Biology* 9 (9): R137.